Impact of hydroxyl functionalization and unsaturation on linear poly(ethylene-co-vinyl alcohol)

Anne N. Radzanowski,[a] Eli J. Fastow,[b] Chien-Hua Tu,[b] James Votruba-Drzal,[b] Vivek Nair,[b]

Karen I. Winey,[b,c,*] E. Bryan Coughlin [a*]

[a] Department of Polymer Science and Engineering, University of Massachusetts Amherst, Amherst, Massachusetts 01003, United States

[b] Department of Material Science and Engineering, University of Pennsylvania, Philadelphia, Pennsylvania 19104, United States

[c] Department of Chemical and Biomolecular Engineering, University of Pennsylvania, Philadelphia, Pennsylvania 19104, United States

Co-Corresponding Authors

* Winey@seas.upenn.edu

* Coughlin@mail.pse.umass.edu

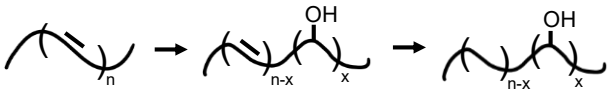

As *x* increases…

Melt Temperature	Increases		Invariant
Crystallinity	Hexagonal		Orthorhombic → Hexagonal
Contact Angle	Decreases		Decreases

Abstract

Functionalization of C=C in unsaturated polyolefins by hydroboration/oxidation successfully generates linear poly(ethylene-*co*-vinyl alcohol) (LEVOH) polymers. This post-polymerization modification expands upon previously reported chemistry to control the extent of functionalization through reagent stoichiometry. Partial functionalization (24 – 92 % of C=C) of polycyclooctene produces materials with both C=C in the backbone and pendant OH, and subsequent hydrogenation generates a LEVOH. We explore the thermal, structural, surface, and adhesive properties of these LEVOH and the partially unsaturated intermediate and find they are impacted by both the extent of OH incorporation and saturation. The presence of C=C significantly reduces the melting temperature and crystallinity while increasing surface polarity and adhesive strength when compared to saturated polymers at equivalent functionalization. This investigation demonstrates linear analogs of EVOH with a wide range of properties tuned by extent of hydroxylation and presence of unsaturation.

Introduction

Poly(ethylene-*co*-vinyl alcohol) (EVOH) is a commercial polyethylene copolymer commonly used in multi-layer packaging. It has utility in multilayer film arises from favorable thermal, adhesive, and oxygen barrier properties.[1] Conventionally synthesized by free radical copolymerization, EVOH is branched with a random comonomer sequence, typically with 52 to 73 mol% vinyl alcohol content, and melting temperatures (T_m) of 157 to 190 °C.[2] Linear analogs to EVOH are well documented to exhibit greater crystallinity, higher melting temperatures, and lower permeability when compared to branched analogs at similar compositions.[3–7]

Linear poly(ethylene-*co*-vinyl alcohol) (LEVOH) are most commonly synthesized by ring-opening metathesis polymerization (ROMP) or acyclic diene metathesis polymerization (ADMET) of pre-functionalized monomers followed by hydrogenation to remove the remaining unsaturation in the backbone inherent to olefin metathesis, **Figure 1**.[3,4,6] The ROMP of cyclooctene has been used to access EVOH copolymers with a maximum of 25 mol% functionalization, defined as the fraction of polyethylene monomeric units with OH groups. Dingwell and Hillmyer generated LEVOH copolymers with 25 mol% functionalization by ROMP of 3- or 5-acetoxy-cyclooctene, followed by hydrogenation and deprotection, to generate LEVOH with either regioregular or regioirregular OH pendant placement. They examined the influence of hydroxyl group regioregularity on crystallinity and permeability.[4,5] X-ray scattering revealed that regioregular EVOH has a monoclinic crystal structure, whereas the regioirregular sample has a hexagonal or pseudo-hexagonal crystal lattice. Similarly, Kennemur and coworkers used ROMP to produce both regioregular, isotactic or atactic, and regioirregular LEVOH (40 mol% functionalization), demonstrating greater crystallinity in the isotactic polymer.[6,7] The regioregular, highly crystalline, and linear EVOH analog prepared by Hillmyer has T_m > 140 °C, while the combination of

regioregularity and isotacticity in the linear EVOH analog prepared by Kennemur has T_m ~ 180 °C.[3-5]

Earlier, Wagener, Saunders Baugh, *et al.* used both ROMP and ADMET to synthesize linear polyethylene copolymers, including LEVOH analogs.[3] Copolymerizing 5-hydroxy-cyclooctene with cyclooctene, the resulting polymers have randomly spaced pendant groups with low, but tailorable, levels of functionalization of 2 - 6 mol%. The melting temperatures and moduli of Wagener's analogs are insensitive to the level of functionalization.[3]

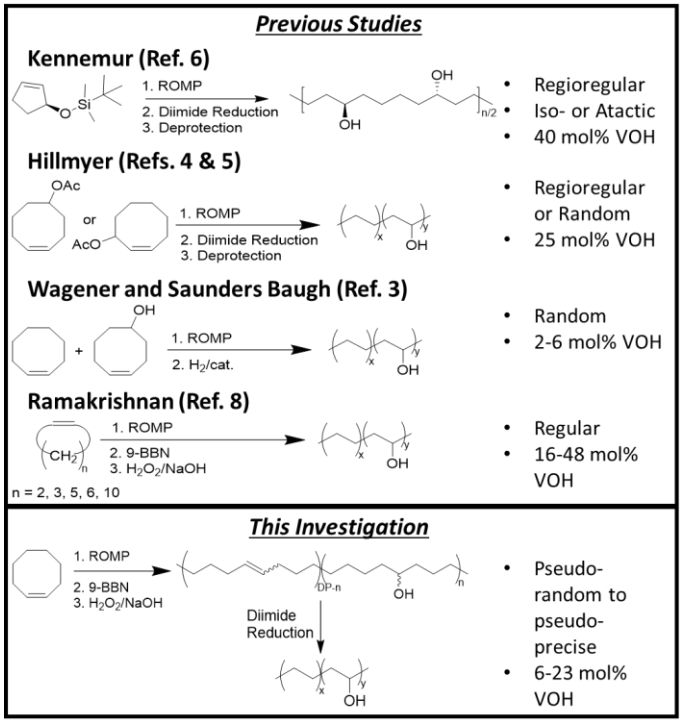

Figure 1. The current investigation explores compositional variations as a function of vinyl alcohol (VOH) content both with and without residual unsaturation.

A third method of accessing linear EVOH analogs is through the post-polymerization modification of polyalkenamers. First reported by Ramakrishnan, complete hydroboration/oxidation of polyalkenamers synthesized from cyclic alkenes of varying ring sizes led to linear EVOH analogs with 16 - 48 mol% functionalization and regular hydroxyl group

spacing, **Figure 1**.[8] All three polymerization approaches can generate an intermediate functional polymer with C=C in the backbone. However, to our knowledge, no published work thoroughly investigates the influence of backbone unsaturation on the properties of linear EVOH analogs.

Motivated by these earlier studies, we examine the influence of both hydroxyl functionalization and unsaturation on the thermal, mechanical, structural, surface, and molecular dynamic properties of novel EVOH analogs. Expanding on Ramakrishnan's study, we employ reagent stoichiometry to achieve fractional hydroboration/oxidation to synthesize pseudo-random to pseudo-precise linear analogs of EVOH and characterize both the unsaturated intermediate and saturated final product.

Materials and Methods

Materials

The following materials were purchased from Sigma Aldrich and used as received: cis-cyclooctene, cis-1,4-dibenzyloxy-2-butene, Grubbs Catalyst® M300, 9-Borabicyclo[3.3.1]nonane solution (0.5 M in THF), tri-*n*-propylamine, *p*-toluenesulfonyl hydrazide, *p*-xylene. The following materials were purchased from Fisher Scientific and used as received: methanol (CH_3OH, ACS Grade), ethanol (CH_3CH_2OH), sodium hydroxide (NaOH, pellets), hydrogen peroxide (H_2O_2, 30% by volume in water), dichloromethane (ACS Grade, DCM). Tetrahydrofuran (THF, ACS Grade) was purified by distillation over sodium benzophenone ketyl radical.

Functionalization of PCOE by hydroboration/oxidation

An oven-dried 3-neck 500 mL round-bottom flask was charged with a stir bar and flame-dried. When just cool, 1.2 g of polycyclooctene (19,000 g/mol, 0.06 mmol) was added to the flask and purged with nitrogen for 10 minutes. Synthesis of PCOE is given in the supporting information. Distilled tetrahydrofuran (THF, to 40 mL total reaction volume) was added to the flask and left to

stir to dissolve the polymer. After 15 minutes of degassing with nitrogen, 9-borabicyclo[3.3.1]nonane solution (9-BBN:olefin molar ratio ranging from 0.5:1 to 1.5:1) was added to the solution. After 5 hours, the flask was moved to an ice bath while retaining stirring and ethanol (EtOH:olefin molar ratio of 37:1) was added dropwise over 5 minutes by syringe to quench any unreacted 9-BBN. Once the ethanol was added, the sodium hydroxide solution (6 M, 11:1 molar ratio NaOH:olefin) was added dropwise over 5 minutes. The hydrogen peroxide solution (30 wt% in H_2O, 33:1 molar ratio H_2O_2:olefin) was added dropwise by syringe over 10 minutes, **Scheme 1**. After 17 hours, the nitrogen purge was stopped and 100 mL of reverse osmosis water was added to the flask. The solution was precipitated in 600 mL of RO water and collected by vacuum filtration. The collected polymer was dried overnight in the vacuum oven at room temperature. These functionalized polymers will be referred to as f(*x*,OH)-PCOE, where *x* is the fraction of ethylene units with OH functionality. These functionalized polymers will be referred to as f(*x*,OH)-PCOE, where *x* is the fraction of ethylene units with OH functionality. Half of the collected polymer was hydrogenated using a diimide reduction as described in the supplemental information. This hydrogenation protocol was first described by Hahn and previously reported for functionalized PCOE.[9–13] The hydrogenated samples are referred to as fh(*x*,OH)-PCOE.

Nuclear magnetic resonance (NMR)

^{1}H and ^{13}C NMR of f(21, OH)-PCOE, f(23, OH)-PCOE, h(0)-HDPE, and all fh(x, OH)-PCOE samples were conducted in 5 mm diameter NMR tubes using 1,1,2,2-tetrachloroethane-d_2 at 100 °C on a Bruker Avance III 600 MHz (150 MHz for ^{13}C) spectrometer. The ^{1}H and ^{13}C NMR of f(6, OH)-PCOE – f(17, OH)-PCOE were conducted in 5 mm diameter NMR tubes using 1,1,2,2-tetrachloroethane-d_2 at 70 °C on a Bruker Avance III 400 MHz (100 MHz for ^{13}C) spectrometer.

The ^{1}H and ^{13}C NMR of PCOE was conducted in a 5 mm diameter NMR tube using $CDCl_3$ at 25 °C a Bruker 500 spectrometer at 500 MHz (125 MHz for ^{13}C).

Differential scanning calorimetry (DSC)

Differential scanning calorimetry (DSC) was performed using a TA Q2000 instrument with ~ 5 mg of polymer powder loaded into hermetic aluminum pans. Samples were subject to an initial heating to 150 °C to erase thermal history followed by a cooling then subsequent heating ramp. The cooling and final heating cycles were conducted with a ramp rate of 10 K/min.

X-ray scattering

Polymers were melt-pressed into flat films approximately 2 cm x 3 cm and 125 μm thick, as measured using a micrometer. Hot pressing of hydrogenated samples proceeded at 135 °C in a custom polytetrafluoroethylene (PTFE) window mold between two liners of PTFE and steel sheets. Pre-hydrogenated samples were hot pressed at T_m + 5 °C to minimize the temperature at which they were exposed to an air atmosphere and reduce the risk of oxidative degradation. After a five-minute pre-heat, polymers were pressed under 1.5 ton of pressure for 15 minutes then allowed to return to room temperature. Hot pressed films were used in X-ray scattering, contact angle, and lap joint shear measurements.

Squares with approximate dimensions of 3 mm x 3 mm were cut from the melt pressed films and affixed to a transmission X-ray scattering stage with Kapton tape. X-ray scattering was performed on a Xeuss 2.0 instrument with a Cu Kα source. Small angle X-ray scattering (SAXS) data were collected by a 1M solid state Pilatus detector and wide-angle X-ray scattering (WAXS) data were collected simultaneously by a 100K Dectris detector. SAXS measurements were performed at a sample to detector (SD) distance of 571 mm and exposure was taken with high flux

collimation (slit 1 at 1.5 mm x 1.5 mm and slit 2 at 0.7 mm x 0.7 mm) for 30 minutes. A Linkam I HFS350 stage was used to control temperature of samples loaded into 1 mm glass capillaries.

Contact angle

Water contact angle measurements were performed by applying a 10 μL droplet to the surface of a hot pressed polymer film. The profile of the droplet was photographed then fit with the Young-Laplace equation to identify contact angle, Eq. S10.[14]

Lap joint shear

Polymers were tested for their adhesive properties using lap joint shear, following ASTM D1002-10.[15] Hot pressed films (300 μm in thickness) were cut into five squares with 1 cm x 1 cm dimensions. These films were placed between two Al coupons in anti-parallel configuration, and the joint was held together with binder clips. The joints were then annealed for 30 minutes at T_m + 5 °C for unsaturated samples or at 135 °C for saturated samples and allowed to cool to room temperature. An Instron Tabletop Universal Testing Machine applied a shear load to the joint at a strain rate of 1.5 mm/min. Ultimate shear stress was taken from the maximum of the resulting stress-strain curves.

Dielectric spectroscopy (DS)

DS measurements were performed using a Solartron 1260 impedance analyzer (12961 dielectric reference module) under continuous vacuum from 183 K to 353 K (precision of ± 0.05K) and in a frequency range of from 10^{-1} to 10^{6} Hz. Sample preparation for DS measurements was done by embedding a thin polymer film between two flat metal electrodes (AFM metal specimen discs, Ted Pella, Inc.) with diameters of 10 mm and 20 mm for top and bottom electrodes, respectively. Thin polymer films with thicknesses 100-200 μm were fabricated by hot pressing (CARVER model 3912) with an applied pressure of 1.2 metric tons at 398 K for 10 minutes. Prior to DS

measurements, the polymer films were annealed overnight (125 °C, vacuum) to eliminate solvent and water. Nonlinear curve fitting to the DS spectra was performed in OriginLab software (OriginPro 2022b). The fitting algorithm uses the Levenberg-Marquardt method with maximum number of fitting iterations and tolerance being set with 500 and 10^{-15}, respectively. The dynamical properties of each relaxation process are extracted via empirical Havriliak-Negami (HN) functions on the imaginary part of the complex dielectric permittivity, Eq. S11.

Results and Discussion

Hydroxylation of PCOE

Post-polymerization modification by a two-step, one-pot hydroboration/oxidation was performed on polycyclooctene (PCOE) to introduce pendant hydroxyl groups. Hydroboration of PCOE with 9-borabicyclo[3.3.1]nonane (9-BBN) was followed by oxidation with sodium hydroxide and hydrogen peroxide, **Scheme 1**. Using PCOE as the starting material, the highest achievable level of functionalization is 25 mol% vinyl alcohol. At low levels of functionalization, the OH groups are distributed along the backbone with a minimum spacing of 6 carbons (pseudo-random), and at nearly 25 mol% functionalization, the OH groups are distributed along the backbone separated by 6, 7, or 8 carbons (pseudo-precise). Post-isolation, half of the recovered material at each level of functionalization was hydrogenated by a diimide reduction to remove the remaining double bonds.[9] The saturated functionalized polymers will be referred to as fh(*x*,OH)-PCOE, where the h denotes complete hydrogenation.

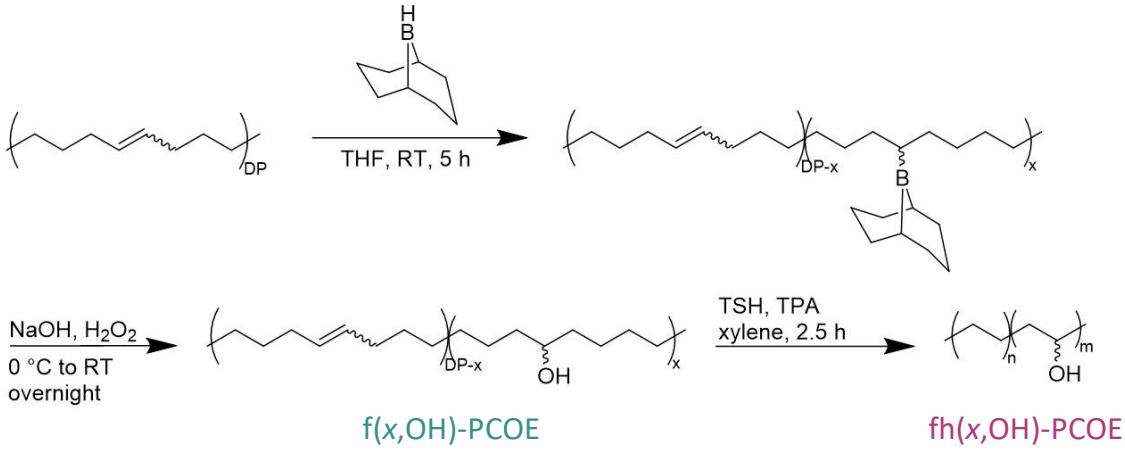

Scheme 1. Hydroboration and oxidation of polycyclooctene followed by hydrogenation using diimide reduction.

The level of functionalization was controlled by varying the ratio of 9-BBN to olefin in the PCOE backbone at a fixed reaction time and polymer concentration, **Figure 2a.** The largest 9-BBN:olefin ratio used was 1.5:1, resulting in 92% conversion of the double bonds, equivalent to 23 mol% functionalization.

Analysis using ^{1}H NMR indicates that the 9-BBN preferentially reacts with the *cis*-double bonds compared to the *trans*-double bonds, as evidenced by the increase in the *trans/cis* ratio in the remaining alkene resonance at ~5.5 ppm with greater functionalization. The ratio between the *trans* and *cis* alkene resonances in the starting polycyclooctene is 62:38 which becomes 77:23 in f(23,OH)-PCOE, **Figure 2b**. Under the reaction conditions employed in these experiments, it is unlikely that *trans/cis* isomerization has occurred.

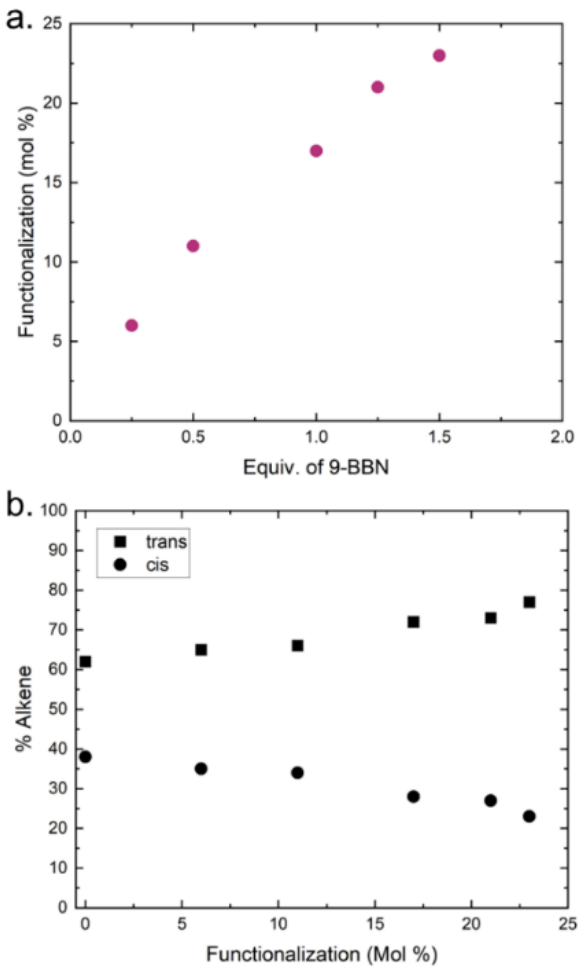

Figure 2. (a.) Functionalization level from ^{1}H-NMR vs ratio of 9-BBN to C=C, and **(b.)** The percentage of *cis* and *trans* double bonds measured by ^{1}H NMR across the range of functionalizations.

Thermal properties and morphology

Both the level of functionalization and the presence of unsaturation were found to tune thermal properties, as measured by differential scanning calorimetry (DSC). However, the glass transition temperature of fh(*x*,OH)-PCOE was invariant across the range of functionalization, matching expectations from Ramakrishnan's studies on linear EVOH, **Figure S13**.[3,4,6,8]

The melting temperatures and crystallinity for f(*x*,OH)-PCOE and fh(*x*,OH)-PCOE were also determined by DSC and strongly depend on both the presence of C=C and functionalization,

Figures 3. In f(*x*,OH)-PCOE, triangles, the melting temperature increases by ~ 70 °C as the level of functionalization increases. This increase in T_m is accompanied by an increase in crystallinity as measured by both DSC and wide-angle X-ray scattering (WAXS), **Figure 3b**. The percent crystallinity from DSC was calculated using a weighted rule of mixtures due to multiple subunits: PCOE, poly(vinyl alcohol), and polyethylene.[4,16] A full description of the calculations can be found in the SI. Crystallinity from WAXS was identified by fitting crystalline peaks with Lorentzian functions and the amorphous halo with a double Gaussian function, then dividing the integrated crystalline intensities by the total intensity (sample fit in **Figure S9**). As OH incorporation increases, Fourier transform infrared (FTIR) spectroscopy reveals an increase in the fraction of alcohol groups within the crystal, **Figure S4-6**. The OH groups within crystallites participate in hydrogen bonding, and these intermolecular attractions reinforce the hexagonally-packed crystallites.[17,18] Thus, we attribute this increase in melting temperature to both higher crystallinity and more hydrogen bonding within the crystals.[19] The T_m range in f(*x*,OH)-PCOE deviates from previous reports of fully saturated linear EVOH analogs, demonstrating the presence of unsaturation disrupts crystallinity and expands the range of accessible melting temperatures.

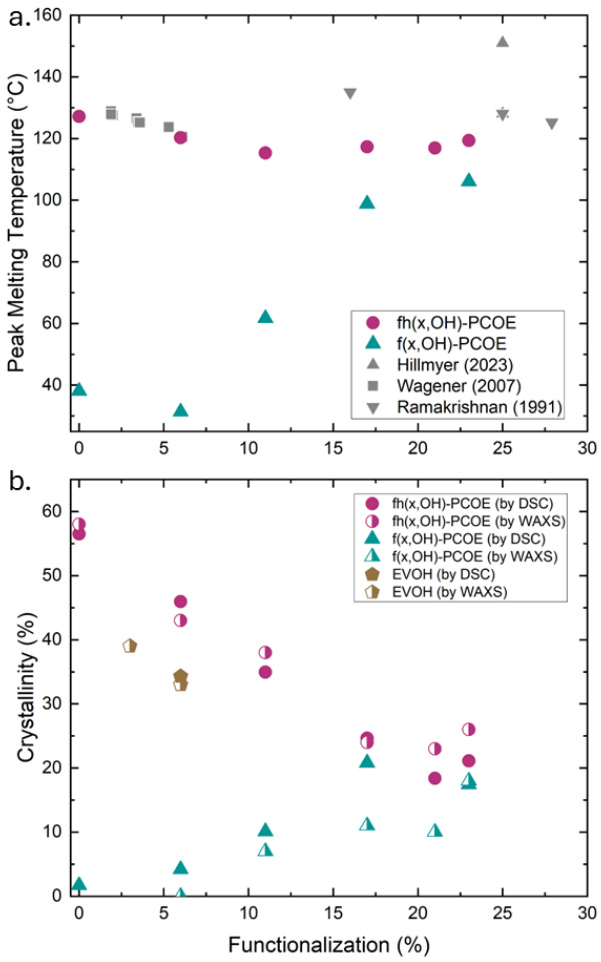

Figure 3. (a) Peak melting temperature determined from the second heating in DSC at 10 K/min and **(b)** crystallinity from DSC (filled) and X-ray scattering (half-filled) plotted against mol % functionalization for f(*x*,OH)-PCOE, fh(*x*,OH)-PCOE, and 3 and 6% commercial EVOH.

The peak melting temperatures of the fh(*x*,OH)-PCOE samples (magenta circles) are insensitive to the level of functionalization, matching prior results from other LEVOHs, **Figure 3a**.[3,4,8] Notably, while the melting temperature spans < 10 °C, the percent crystallinity substantially decreases from ~ 58% to ~ 20%, **Figure 3b**. We attribute the T_m trend observed in fh(*x*,OH)-PCOE to the confluence of a loss of crystallinity (expected to decrease T_m) and an increase in hydrogen bonding within crystals (expected to increase T_m). In the saturated polymers, crystallinity decreases with greater functionalization but does not disappear, consistent with the trend observed by prior

investigations into EVOH copolymers.[3,20] Notably, the crystallinity of fh(*x*,OH)-PCOE exceeds that of random and branched EVOH by ~ 15 % at the same level of functionalization (3 – 6 %), **Figure 3b**. As permeability decreases with crystallinity, this disparity motivates additional investigations into the crystallization and permeability behavior of fh(*x*,OH)-PCOE, which are ongoing.[1,21,22] We expect the difference in chain architecture (between linear and branched) and OH content to play a significant role in both the total crystallinity and crystallization kinetics.

Prior studies on branched EVOHs with random distributions of OH groups reveal a transition from orthorhombic to hexagonal to monoclinic crystal structures as OH content increases.[18,23] As measured on random EVOH, the crystal structure transitions from orthorhombic to hexagonal at ~ 17 - 20 mol% OH and from hexagonal to monoclinic at > 25 mol%.[4,18,23,24] Hillmyer reported that regioregular EVOH exhibits a monoclinic structure at 25 mol% vinyl alcohol incorporation, while the regiorandom analog exhibits a hexagonal structure at the same composition.[4] In fh(*x,*OH)-PCOE, X-ray scattering measurements show a transition in crystal structure from orthorhombic to hexagonal as functionalization level increases, **Figure 4b**. This matches prior measurements of both random and pseudo-precise EVOH.[4,25,26]

In contrast, the f(*x*,OH)-PCOE samples exhibit hexagonal crystal structures at $x \geq 11$ mol%, **Figure 4a**. Though prior investigations of the PCOE structure identified a triclinic crystal lattice,[10,27,28] the X-ray scattering data are inconsistent with triclinic structure in f(*x*,OH)-PCOE. Evidently, even low levels of OH incorporation disrupt PCOE crystallization. Thus, we attribute the crystallization in unsaturated samples to the presence of OH groups driving crystallization in a hexagonal crystal structure, similar to saturated EVOH with moderate OH incorporation.[18,23]

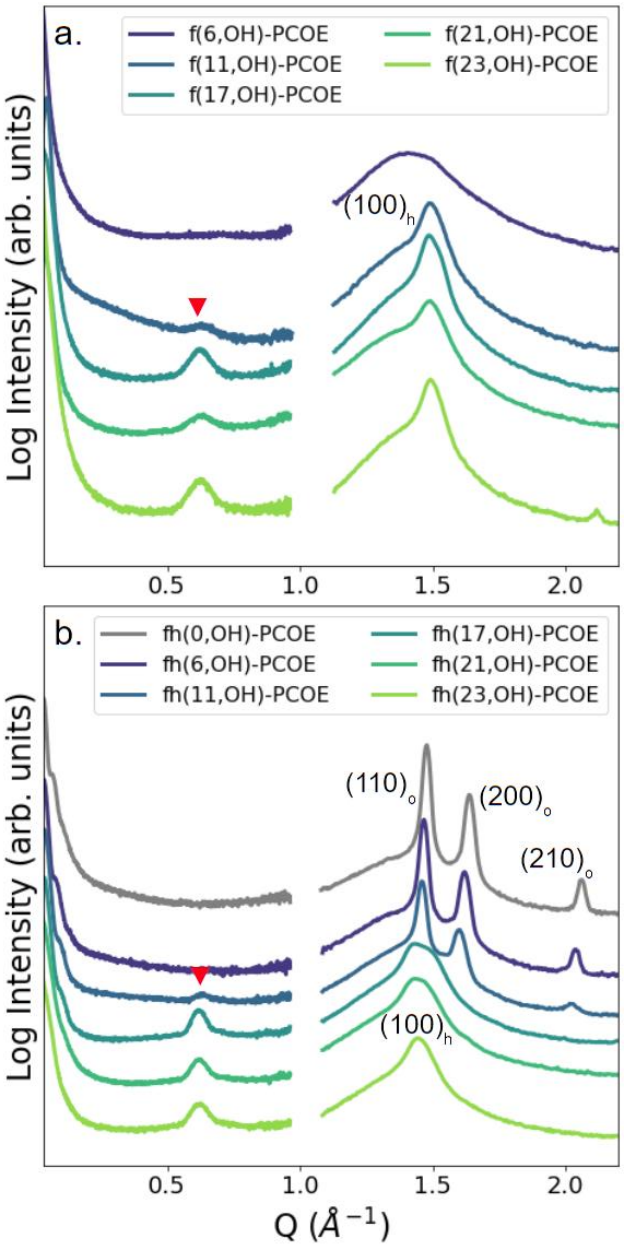

Figure 4. X-ray scattering of **(a)** unsaturated f(*x*,OH)-PCOE polymers and **(b)** saturated fh(*x*,OH)-EVOH polymers. The peak at ~0.6 $Å^{-1}$ (▼) is attributed to scattering between OH groups in crystallites and the features at Q > 1 $Å^{-1}$ indicate both the amorphous and crystalline domains, where subscripts h and o indicate hexagonal and orthorhombic lattices.

The scattering feature at Q ~ 0.6 $Å^{-1}$ in both the unsaturated and saturated polymers corresponds to the distance between OH groups within crystals with a characteristic spacing of ~ 10 Å. As the OH can add to either carbon in the C=C, at complete conversion alcohols are separated by 7 to 9

C-bonds, which corresponds to 8.80 to 11.31 Å between OH groups assuming an all *trans* polymer conformation, **Figure 5d**. This is consistent with the peak assignment, which is further supported by X-ray scattering at $T > T_m$ where the peak at Q ~ 0.6 $Å^{-1}$ is absent, **Figure S7**.[4,26] Additionally, X-ray scattering of fh(23,OH)-PCOE strained beyond the yield point reveals this small angle peak orients orthogonal to the crystalline peak, supporting the assignment of this peak to OH-to-OH separation in the crystal, **Figure S8**. The lack of detectable higher order peaks, even upon drawing, indicates the OH groups do not form well-ordered layers as reported in other functionalized polyethylenes with precise separations between functional groups.[29–32]

Surface and adhesive properties

The water contact angles were determined by fitting the Young-Laplace equation to an image of a water droplet on a hot pressed polymer film, **Figure 5a**.[33] The contact angle decreases with increasing functionalization, from 112.4 ± 3.5° in fh(0,OH)-PCOE to 75.7 ± 1.4° for f(23,OH)-PCOE and 85.2 ± 2.6° for fh(23,OH)-PCOE. Also, at all levels of functionalization, the unsaturated samples exhibit lower contact angles, indicating a more polar surface, than the saturated polymers. We ascribe this difference in surface polarity between saturated and unsaturated samples to the OH groups available to form hydrogen bonds at the surface. Note that OH groups within crystals are unavailable to participate in polar interactions at the surface.[17,18] The fraction of OH groups in the amorphous phase varies with the level of functionalization and the presence of C=C, as determined by FTIR (**Figures S4-S6**). The more crystalline fh(*x*,OH)-PCOE polymers have fewer OH groups in the amorphous phase that leads to higher contact angles, **Figure 5b**. Note that the contact angle correlates better with the amount of amorphous phase OH (**Figure 5b**) than the level of functionalization (**Figure 5a**).

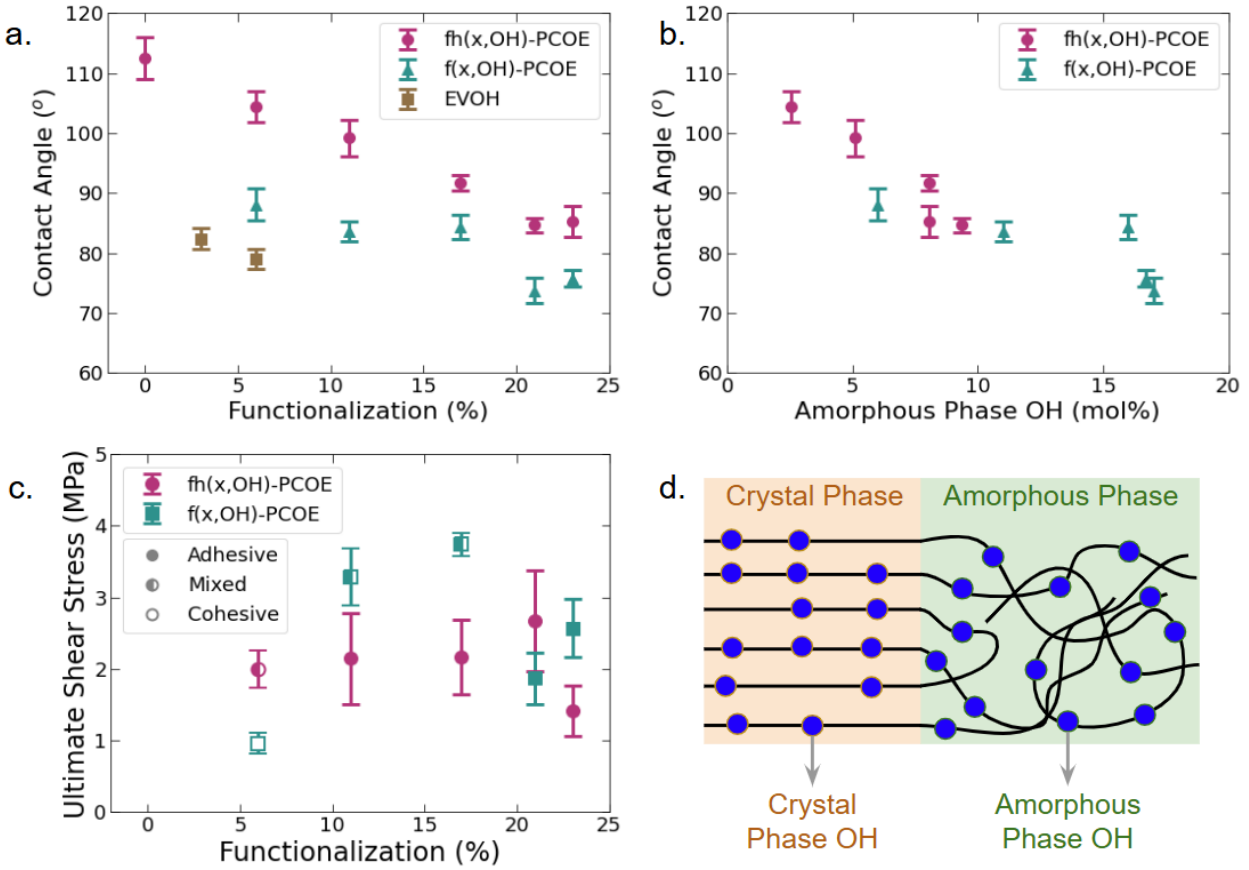

Figure 5. Water contact angle decreases with **(a)** functionalization (*x*) and **(b)** amorphous phase composition (mol% OH) in f(*x*,OH)-PCOE, fh(*x*,OH)-PCOE, and EVOH. **(c)** Ultimate shear stress where filled, half-filled and open symbols represent adhevise, mixed and cohesive failure, respectivley. **(d)** Schematic of fh(*x*,OH)-PCOE showing a semicrystalline morphology with OH groups distributed between the crystalline and amorphous phases.

At high levels of functionalization (> 12 mol %), both the unsaturated and saturated samples achieve contact angles similar to commercial EVOH with 6 mol% OH, **Figure 5a**. We attribute the difference between the contact angles of 6 mol% EVOH and fh(6,OH)-PCOE to the greater mobility and reduced crystallinity inherent to branched polymer architectures. Greater branching increases the free volume, increasing polymer mobility and enabling the OH groups in commercial EVOH to segregate to the surface.[34–36] Additionally, with less crystallinity than fh(6,OH)-PCOE,

more OH groups are in the amorphous region and available to form hydrogen bonds at the surface, thus decreasing the contact angle.

Lap joint shear measurements characterized the adhesive properties of both the unsaturated and saturated polymers, and stress-strain curves are shown in **Figure S15**.[15] The measured ultimate shear stress (USS) reaches a maximum of 3.28 ± 0.40 MPa in f(17,OH)-PCOE, **Figure 5c**. This value demonstrates the polymers reported here have sufficient strength in an adhesive configuration for commercial applications.[10] Given that the entanglement molecular weight of EVOH is reported to be similar to polyethylene (M_e = ~ 1.1 kg/mol) and the molecular weights of the LEVOHs studied here are 2.5 – 6.6 times larger, we expect the T_g, T_m, crystal structures, contact angles and segmental dynamics to be similar for higher molecular weight LEVOHs. In contrast, the adhesive properties of LEVOH are likely to improve with increasing molecular weight.[38]

The USS of unsaturated samples exhibits three failure modes: cohesive, mixed, and adhesive. Cohesive failure in f(6,OH)-PCOE is attributed to low bulk strength as a consequence of low crystallinity, consistent with previously observed loss of bulk strength with a decrease in crystallinity in hydroxyl-functionalized PCOE.[10] As the crystallinity increases with functionalization in f(*x*,OH)-PCOE, the failure mode shifts to mixed then adhesive. The measured USS of fh(*x*,OH)-PCOE samples does not meaningfully change with respect to functionalization. Changes to the crystal structure from orthogonal to hexagonal with increasing *x* favors the inclusion of OH groups in the crystal, decreasing the fraction of OH in the amorphous regime, **Figure S5**.[17,18,39] Fewer OH groups in the amorphous regime only modestly impact the adhesive properties.

Polymer dynamics

Local dynamics of f(*x*,OH)-PCOE and fh(*x*,OH)-PCOE were investigated by dielectric spectroscopy (DS) to produce relaxation maps, **Figure 6**. Relaxation times were extracted from dielectric loss spectra fit to the Havriliak-Negami function, **Figures S16** and **S17**. In **Figure 6a**, the α-process significantly slows with decreasing temperature across the entire temperature range, following Vogel-Fulcher-Tammann (VFT) behavior that implies coordinated motion. The agreement between the T_g from DS (VFT extrapolation to τ~100s) and DSC supports assignment of the dielectric α-process as segmental dynamics. In **Figure 6b**, the β-process shows a weaker temperature dependence and follows Arrhenius behavior. The E_a values for the β-processes are relatively small (8 – 18 kJ/mol, **Table S7**), and are most likely due to the motions at length scales much smaller than segments. Note the dynamics detected by DS are specific to the mobile polymer chains and free ends (dielectrically active) in the amorphous domain (see inset, **Figure 6a**). Upon saturation, we observe slower segmental and faster sub-segmental dynamics, suggesting the absence of C=C on the polymer chain backbone decreases mobility in the rubbery regime but increases mobility in the glassy regime. Oxygen permeability is known to increase with free volume in the amorphous domain, and free volume has been shown to increase with greater mobility in amorphous polymer.[40–43]

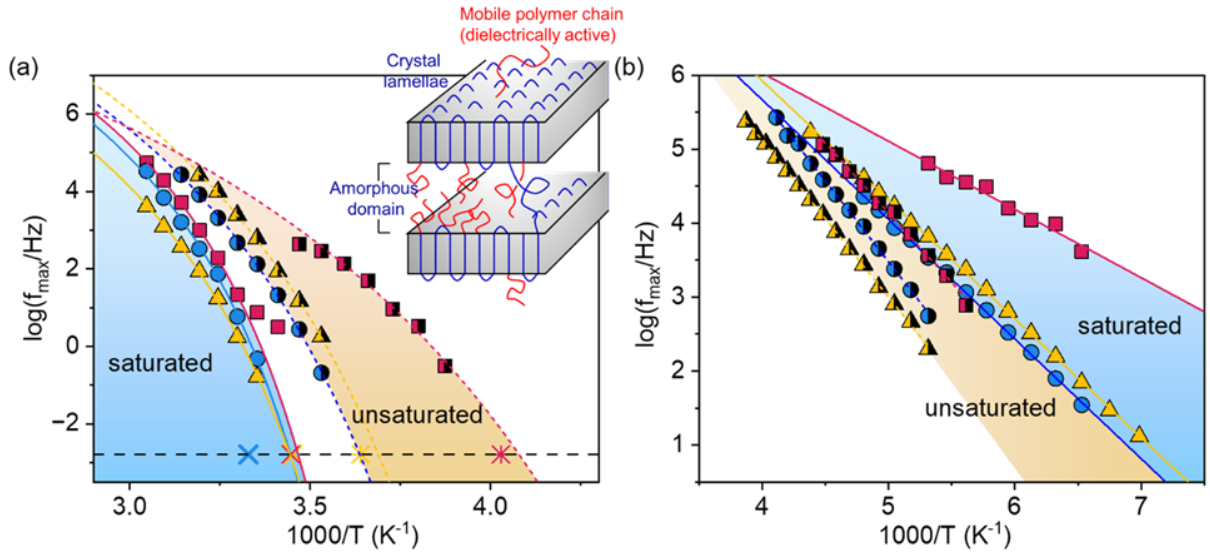

Figure 6. Relaxation map for the **(a)** α- and **(b)** β-processes in the f(x,OH)-PCOE (half-filled symbols) and fh(x,OH)-PCOE (filled symbols), x = 11 mol% (magenta square), 17 mol% (yellow triangle), and 21 mol% (blue sphere). The curved lines show **(a)** VFT fittings and **(b)** Arrhenius fitting. The inset illustrates that only polymer segments with amorphous domain are dielectrically active. In **(a)** crosses and asterisks give T_g from DSC (crosses for saturated and asterisks for unsaturated) and the horizontal black dashed line indicates a relaxation time of ~ 100s [log(f/Hz) ~ -2.79]. A T_g value is not available for f(21,OH)-PCOE.

Conclusion

Post-polymerization functionalization of polycyclooctene was accomplished with fractional hydroboration/oxidation, resulting in linear EVOH polymers. The level of functionalization was well-controlled by varying the stoichiometric ratio between 9-BBN and C=C along the polymer backbone. We investigated both the saturated LEVOH, and unsaturated intermediates, and found that both the extent of functionalization and presence of C=C tune thermal, morphological, surface, mechanical, and dynamic properties. Unsaturated f(x,OH)-PCOE polymers show an increase in melting temperature and crystallinity with increasing functionalization. This contrasts with a near invariant melting temperature (~120 °C) and a decrease in crystallinity with increasing OH content in the fh(x,OH)-PCOE polymers. Additionally, fh(x,OH)-PCOE exhibits greater crystallinity than f(x,OH)-PCOE at all levels of functionalization, and the saturated LEVOH exhibits a transition in

crystal structure (from orthorhombic to hexagonal) with greater OH incorporation absent in the purely hexagonal unsaturated LEVOH. The difference in morphology between these two materials led to a disparity in the distribution between OH groups across the amorphous and crystalline regimes, explaining the higher surface polarity exhibited by f(*x*,OH)-PCOE. Varying OH incorporation and unsaturation tunes the contact angle, adhesion, and polymer mobility properties of LEVOH, widening the envelope of observed properties when compared to previously reported EVOHs. Future studies will explore the crystallization kinetics and the oxygen permeability of these LEVOHs. The role of molecular weight on properties of these LEVOHs is left for future investigations.

ASSOCIATED CONTENT

Supporting Information. Supporting information contains additional experimental materials and measurements of each sample by: ^{1}H NMR, FTIR, DSC, X-ray scattering, contact angle, lap joint shear, and dielectric spectroscopy.

AUTHOR INFORMATION

Corresponding Authors

Karen I. Winey - Department of Chemical and Biomolecular Engineering, Department of Materials Science and Engineering, University of Pennsylvania, Philadelphia, Pennsylvania 19104, United States; orcid.org/0000-0001-5856-3410; Email: winey@ seas.upenn.edu

E. Bryan Coughlin – Department of Polymer Science and Engineering, University of Massachusetts Amherst, Amherst, Massachusetts 01003, United States; orcid.org/0000-0001-7065-4366

Authors

Anne N. Radzanowski − Department of Polymer Science and Engineering, University of Massachusetts Amherst, Amherst, Massachusetts 01003, United States; orcid.org/0000-0001-6453-3103

Eli J. Fastow − Department of Materials Science and Engineering, University of Pennsylvania, Philadelphia, Pennsylvania 19104, United States; orcid.org/00000003-2674-2056

Chien-Hua Tu − Department of Materials Science and Engineering, University of Pennsylvania, Philadelphia, Pennsylvania 19104, United States; orcid.org/0000-0002-8351-7130

James Votruba-Drzal − Department of Materials Science and Engineering, University of Pennsylvania, Philadelphia, Pennsylvania 19104, United States; orcid.org/0009-0007-7048-9445

Vivek Nair − Department of Materials Science and Engineering, University of Pennsylvania, Philadelphia, Pennsylvania 19104, United States; orcid.org/0009-0002-0858-3565

Author Contributions

CRediT: Anne N. Radzanowski data curation, formal analysis, investigation, methodology, visualization, writing original draft; Eli J. Fastow data curation, formal analysis, investigation, methodology, visualization, writing-original draft; Chien-Hua Tu data curation, formal analysis, investigation, methodology, visualization, writing-original draft; James Votruba-Drzal data curation, formal analysis, investigation; Vivek Nair data curation, formal analysis, investigation; Karen I. Winey conceptualization, funding acquisition, project administration, supervision, writing-review & editing; E. Bryan Coughlin conceptualization, funding acquisition, project administration, supervision, writing-review & editing.

Funding Sources

The authors gratefully acknowledge funding by DOE BES (DESC0022238).

Notes

The authors declare no competing financial interests.

ACKNOWLEDGMENT

The authors gratefully acknowledge funding by DOE BES (DESC0022238). The authors also wish to acknowledge Steve Szewczyk for his assistance with the DSC system and Dr. Weiguo Hu for his assistance with the NMR measurements. E.J.F. and K.I.W. acknowledge use of the Dual Source and Environmental X-ray Scattering facility operated by the Laboratory for Research on the Structure of Matter at the University of Pennsylvania supported by NSF through DMR-2309043 grant. E.J.F. acknowledges support from the Vagelos Institute of Energy Sciences and Technology in the form of a graduate fellowship.

References

(1) Maes, C.; Luyten, W.; Herremans, G.; Peeters, R.; Carleer, R.; Buntinx, M. Recent Updates on the Barrier Properties of Ethylene Vinyl Alcohol Copolymer (EVOH): A Review. *Polym. Rev.* **2018**, *58* (2), 209–246. https://doi.org/10.1080/15583724.2017.1394323.

(2) Kuraray. *Kuraray - EVAL™ EVOH*. Kuraray. https://eval.kuraray.com/ (accessed 2023-09-17).

(3) Lehman, S. E. Jr.; Wagener, K. B.; Baugh, L. S.; Rucker, S. P.; Schulz, D. N.; Varma-Nair, M.; Berluche, E. Linear Copolymers of Ethylene and Polar Vinyl Monomers via Olefin Metathesis−Hydrogenation: Synthesis, Characterization, and Comparison to Branched Analogues. *Macromolecules* **2007**, *40* (8), 2643–2656. https://doi.org/10.1021/ma070085p.

(4) Dingwell, C. E.; Hillmyer, M. A. Regiospecific Poly(Ethylene-Co-Vinyl Alcohol) by ROMP of 3-Acetoxycyclooctene and Postpolymerization Modification for Barrier Material Applications. *ACS Appl. Polym. Mater.* **2023**, *5* (3), 1828–1836. https://doi.org/10.1021/acsapm.2c01918.

(5) Dingwell, C. E.; Hillmyer, M. A. Regio- and Stereoregular EVOH Copolymers from ROMP as Designer Barrier Materials. *ACS Polym. Au* **2024**. *4* (*3*) 208 - 213 https://doi.org/10.1021/acspolymersau.4c00006.

(6) Guillory, G. A.; Marxsen, S. F.; Alamo, R. G.; Kennemur, J. G. Precise Isotactic or Atactic Pendant Alcohols on a Polyethylene Backbone at Every Fifth Carbon: Synthesis, Crystallization, and Thermal Properties. *Macromolecules* **2022**, *55* (15), 6841–6851. https://doi.org/10.1021/acs.macromol.2c01090.

(7) Tashiro, K.; Guillory, G. A.; Marxsen, S. F.; Kennemur, J. G.; Alamo, R. G. Crystal Structures of Isotactic and Atactic Poly(1-Pentamethylene Alcohol). *Macromolecules* **2023**, *56* (15), 5993–6002. https://doi.org/10.1021/acs.macromol.3c01060.

(8) Ramakrishnan, S. Well-Defined Ethylene-Vinyl Alcohol Copolymers via Hydroboration: Control of Composition and Distribution of the Hydroxyl Groups on the Polymer Backbone. *Macromolecules* **1991**, *24* (13), 3753–3759. https://doi.org/10.1021/ma00013a003.

(9) Hahn, S. F. An Improved Method for the Diimide Hydrogenation of Butadiene and Isoprene Containing Polymers. *J. Polym. Sci. A Polym. Chem.* **1992**, *30* (3), 397–408. https://doi.org/10.1002/pola.1992.080300307.

(10) Chethalen, R. J.; Fastow, E. J.; Coughlin, E. B.; Winey, K. I. Thiol–Ene Click Chemistry Incorporates Hydroxyl Functionality on Polycyclooctene to Tune Properties. *ACS Macro Lett.* **2023**, *12* (1), 107–112. https://doi.org/10.1021/acsmacrolett.2c00670.

(11) Fastow, E.; Chethalen, R. J.; Coughlin, E. B.; Winey, K. I. Thiol-Ene Click Chemistry Incorporates Carboxylic Acid-Terminated Alkane Pendants on Polycyclooctene to Tune Properties. *Giant* **2024**, *17*, 100231. https://doi.org/10.1016/j.giant.2023.100231.

(12) Ogbu, I. M.; Fastow, E. J.; Zhu, W.; Wells, L. A.; Chethalen, R. J.; Nair, V.; Hinton, Z. R.; Balzer, A. H.; Hu, W.; Coughlin, E. B.; Winey, K. I.; Kozlowski, M. C. Hydrocarboxylation of C═C Bonds in Polycyclooctene: Progress Toward Valorization of Waste Polyolefins. *Macromolecules* **2024**. https://doi.org/10.1021/acs.macromol.4c00771.

(13) Ogbu, I. M.; Fastow, E. J.; Winey, K. I.; Kozlowski, M. C. Hydroesterification of Polycyclooctene to Access Linear Ethylene Ethyl Acrylate Copolymers as a Step Toward Polyolefin Functionalization. *Macromolecules* **2024**. https://doi.org/10.1021/acs.macromol.4c02074.

(14) Stadler, F. J.; Bailly, C. A New Method for the Calculation of Continuous Relaxation Spectra from Dynamic-Mechanical Data. *Rheol. Acta* **2009**, *48* (1), 33–49. https://doi.org/10.1007/s00397-008-0303-2.
(15) D14 Committee. *Test Method for Apparent Shear Strength of Single-Lap-Joint Adhesively Bonded Metal Specimens by Tension Loading (Metal-to-Metal)*; ASTM International. https://doi.org/10.1520/D1002-10R19.
(16) Faisant, J. B.; Aït-Kadi, A.; Bousmina, M.; Descheˆnes, L. Morphology, Thermomechanical and Barrier Properties of Polypropylene-Ethylene Vinyl Alcohol Blends. *Polym.* **1998**, *39* (3), 533–545. https://doi.org/10.1016/S0032-3861(97)00313-3.
(17) Xu, W.; Asai, S.; Sumita, M. Spectroscopic Study of Ethylene Vinyl Alcohol Copolymer and Poly (Vinyl Alcohol). *SEN'I GAKKAISHI* **1997**, *53* (5), 174–182. https://doi.org/10.2115/fiber.53.5_174.
(18) Takahashi, M.; Tashiro, K.; Amiya, S. Crystal Structure of Ethylene−Vinyl Alcohol Copolymers. *Macromolecules* **1999**, *32* (18), 5860–5871. https://doi.org/10.1021/ma990521a.
(19) Crist, B. Thermodynamics of Statistical Copolymer Melting. *Polymer* **2003**, *44* (16), 4563–4572. https://doi.org/10.1016/S0032-3861(03)00331-8.
(20) Alvarez, V. A.; Kenny, J. M.; Vázquez, A. Isothermal Crystallization of Poly(Vinyl Alcohol–Co–Ethylene). *J. of Appl. Polym. Sci.* **2003**, *89* (4), 1071–1077. https://doi.org/10.1002/app.12255.
(21) Lagaron, J. M.; Catalá, R.; Gavara, R. Structural Characteristics Defining High Barrier Properties in Polymeric Materials. *Matl. Sci. and Tech.* **2004**, *20* (1), 1–7. https://doi.org/10.1179/026708304225010442.
(22) Lee, S. Y.; Kim, S. C. Laminar Morphology Development and Oxygen Permeability of LDPE/EVOH Blends. *Polym. Eng. & Sci.* **1997**, *37* (2), 463–475. https://doi.org/10.1002/pen.11690.
(23) Matsumoto T.; Nakamae K.; Kogoshi N.; Kawazoe M.; Oka H. Crystallinity of ethylene-vinyl alcohol copolymer. 高分子化學 **1971**, *28* (315), 610-617,647. https://doi.org/10.1295/koron1944.28.610.
(24) Bunn, C. W. Crystal Structure of Polyvinyl Alcohol. *Nature* **1948**, *161* (4102), 929–930. https://doi.org/10.1038/161929a0.
(25) Watson, M. D.; Wagener, K. B. Ethylene/Vinyl Acetate Copolymers via Acyclic Diene Metathesis Polymerization. Examining the Effect of "Long" Precise Ethylene Run Lengths. *Macromolecules* **2000**, *33* (15), 5411–5417. https://doi.org/10.1021/ma9920689.
(26) Zhang, J.; Matta, M. E.; Martinez, H.; Hillmyer, M. A. Precision Vinyl Acetate/Ethylene (VAE) Copolymers by ROMP of Acetoxy-Substituted Cyclic Alkenes. *Macromolecules* **2013**, *46* (7), 2535–2543. https://doi.org/10.1021/ma400092z.
(27) Bassi, I. W.; Fagherazzi, G. The Triclinic Structure of Trans-Polyoctenamer. *Euro. Polym. J.* **1968**, *4* (1), 123–132. https://doi.org/10.1016/0014-3057(68)90013-X.
(28) Liu, C.; Chun, S. B.; Mather, P. T.; Zheng, L.; Haley, E. H.; Coughlin, E. B. Chemically Cross-Linked Polycyclooctene: Synthesis, Characterization, and Shape Memory Behavior. *Macromolecules* **2002**, *35* (27), 9868–9874. https://doi.org/10.1021/ma021141j.
(29) Middleton, L. R.; Szewczyk, S.; Azoulay, J.; Murtagh, D.; Rojas, G.; Wagener, K. B.; Cordaro, J.; Winey, K. I. Hierarchical Acrylic Acid Aggregate Morphologies Produce Strain-Hardening in Precise Polyethylene-Based Copolymers. *Macromolecules* **2015**, *48* (11), 3713–3724. https://doi.org/10.1021/acs.macromol.5b00797.

(30) Middleton, L. R.; Winey, K. I. Nanoscale Aggregation in Acid- and Ion-Containing Polymers. *Annu. Rev. Chem. Biomol. Eng.* **2017**, *8* (1), 499–523. https://doi.org/10.1146/annurev-chembioeng-060816-101531.
(31) Middleton, L. R.; Trigg, E. B.; Schwartz, E.; Opper, K. L.; Baughman, T. W.; Wagener, K. B.; Winey, K. I. Role of Periodicity and Acid Chemistry on the Morphological Evolution and Strength in Precise Polyethylenes. *Macromolecules* **2016**, *49* (21), 8209–8218. https://doi.org/10.1021/acs.macromol.6b00937.
(32) Trigg, E. B.; Middleton, L. R.; Moed, D. E.; Winey, K. I. Transverse Orientation of Acid Layers in the Crystallites of a Precise Polymer. *Macromolecules* **2017**, *50* (22), 8988–8995. https://doi.org/10.1021/acs.macromol.7b02094.
(33) Stalder, A. F.; Melchior, T.; Müller, M.; Sage, D.; Blu, T.; Unser, M. Low-Bond Axisymmetric Drop Shape Analysis for Surface Tension and Contact Angle Measurements of Sessile Drops. *Colloids and Surfaces A: Physicochemical and Engineering Aspects* **2010**, *364* (1–3), 72–81. https://doi.org/10.1016/j.colsurfa.2010.04.040.
(34) Fetters, L. J.; Lohse, D. J.; Richter, D.; Witten, T. A.; Zirkel, A. Connection between Polymer Molecular Weight, Density, Chain Dimensions, and Melt Viscoelastic Properties. *Macromolecules* **1994**, *27* (17), 4639–4647. https://doi.org/10.1021/ma00095a001.
(35) Luo, X.; Xie, S.; Liu, J.; Hu, H.; Jiang, J.; Huang, W.; Gao, H.; Zhou, D.; Lü, Z.; Yan, D. The Relationship between the Degree of Branching and Glass Transition Temperature of Branched Polyethylene: Experiment and Simulation. *Polym. Chem.* **2014**, *5* (4), 1305–1312. https://doi.org/10.1039/C3PY00896G.
(36) López-Barrón, C. R.; Tsou, A. H.; Hagadorn, J. R.; Throckmorton, J. A. Highly Entangled α-Olefin Molecular Bottlebrushes: Melt Structure, Linear Rheology, and Interchain Friction Mechanism. *Macromolecules* **2018**, *51* (17), 6958–6966. https://doi.org/10.1021/acs.macromol.8b01431.
(37) Ketels, H. H. T. M. Synthesis, Characterization and Applications of Ethylene Vinylalcohol Copolymers. Phd Thesis 1 (Research TU/e / Graduation TU/e), Technische Universiteit Eindhoven, Eindhoven, 1989. https://doi.org/10.6100/IR316591.
(38) Nunes, R. W.; Martin, J. R.; Johnson, J. F. Influence of Molecular Weight and Molecular Weight Distribution on Mechanical Properties of Polymers. *Polym. Eng. & Sci.* **1982**, *22* (4), 205–228. https://doi.org/10.1002/pen.760220402.
(39) Tashiro, K.; Sasaki, S.; Kobayashi, M. Structural Investigation of Orthorhombic-to-Hexagonal Phase Transition in Polyethylene Crystal: The Experimental Confirmation of the Conformationally Disordered Structure by X-Ray Diffraction and Infrared/Raman Spectroscopic Measurements. *Macromolecules* **1996**, *29* (23), 7460–7469. https://doi.org/10.1021/ma960333+.
(40) Ito, K.; Saito, Y.; Yamamoto, T.; Ujihira, Y.; Nomura, K. Correlation Study between Oxygen Permeability and Free Volume of Ethylene−Vinyl Alcohol Copolymer through Positronium Lifetime Measurement. *Macromolecules* **2001**, *34* (18), 6153–6155. https://doi.org/10.1021/ma001813a.
(41) Frisch, L. Fundamentals of Membrane Transport. *Polym. J.* **1991**, *23* (5).
(42) Turnbull, D.; Cohen, M. H. Free-Volume Model of the Amorphous Phase: Glass Transition. *J. of Chem. Phys.* **1959**, *31* (5).
(43) White, R. P.; Lipson, J. E. G. A Simple New Way To Account for Free Volume in Glassy Dynamics: Model-Free Estimation of the Close-Packed Volume from PVT Data. *J. Phys. Chem. B* **2021**, *125* (16), 4221–4231. https://doi.org/10.1021/acs.jpcb.1c01620.

Supporting Information

Impact of hydroxyl functionalization and unsaturation on linear poly(ethylene-co-vinyl alcohol)

Anne N. Radzanowski,[a] Eli J. Fastow,[b] Chien-Hua Tu,[b] James Votruba-Drzal,[b] Vivek Nair,[b]

Karen I. Winey,[b,c,*] E. Bryan Coughlin [a*]

[a] Department of Polymer Science and Engineering, University of Massachusetts Amherst, Amherst, Massachusetts 01003, United States

[b] Department of Material Science and Engineering, University of Pennsylvania, Philadelphia, Pennsylvania 19104, United States

[c] Department of Chemical and Biomolecular Engineering, University of Pennsylvania, Philadelphia, Pennsylvania 19104, United States

Email: Winey@seas.upenn.edu
Email: Coughlin@mail.pse.umass.edu

Contents:

Synthesis of Polycyclooctene

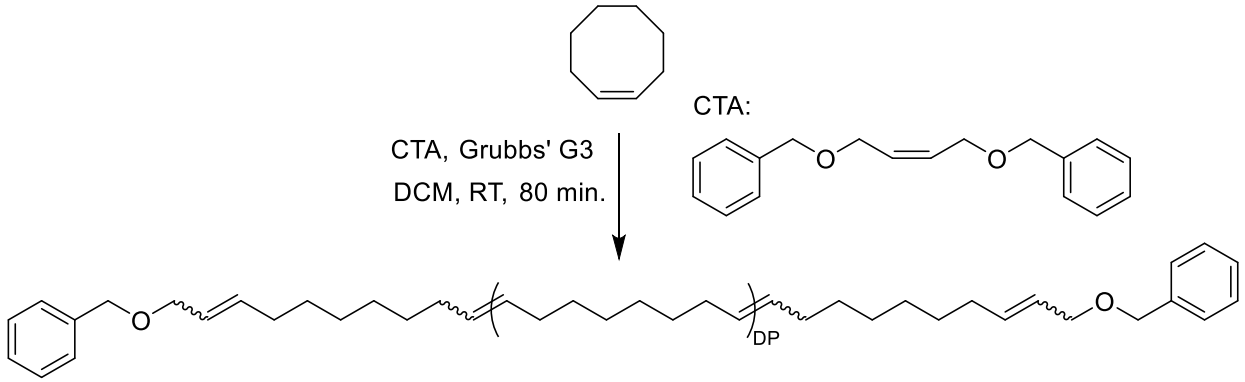

Scheme S1. Synthesis of polycyclooctene using Grubbs' Generation 3 catalyst and cis-1,4-dibenzyloxy-2-butene as the chain transfer agent.

Cis-cyclooctene (20 mL, 0.15 mol) and dichloromethane (35 mL) were added to a 2-neck round-bottom flask and placed under a nitrogen purge for 10 minutes. Cis-1,4-dibenzyloxy-2-butene (1.66 g, 6.2 mmol) was added to the flask by syringe. Grubbs' Generation 3 catalyst (M300, 0.019 g, 0.02 mmol) was dissolved in 1 mL of DCM and added to the flask by syringe, **Scheme S1**. When the viscosity of the solution increased, it was diluted with 10 mL additional DCM to maintain stirring. After 80 minutes, the reaction was quenched with ethyl vinyl ether (0.2 mL, 0.2 mmol) and precipitated in 8x by volume stirred methanol. The precipitated polymer was collected by vacuum filtration and dried overnight at room temperature in the vacuum oven. The isolated yield was 16.83 g, M_w by GPC was 29,200 g/mol, M_n by GPC was 18,700 g/mol, and the dispersity (Đ) was 1.56. The M_n by NMR end-group analysis was 5,700 g/mol.

Hydrogenation of PCOE and Functionalized PCOE by Diimide Reduction

A polymer f(*x*, OH)-PCOE (0.75 g, 4.01×10^{-5} mol) was added to a 3-neck round-bottom flask and dissolved in *p*-xylene (to 25 weight % solids) at room temperature for 15 minutes while degassing with nitrogen, **Scheme 1**. After 15 minutes, the flask was moved to a 125 ˚C oil bath where degassing continued for 10 minutes while the oil bath returned to temperature. Tri-*n*-propyl amine (TPA, TPA:olefin molar ratio 6:1) was added to the flask by syringe and left to stir for five minutes, following the procedure developed by Hahn *et al*.[1] One third, by volume, of the *p*-toluenesulfonyl hydrazide (TSH) (TSH:olefin molar ratio 6:1) was added to the reaction. The remaining two-thirds of the TSH were added in 10-minute increments. After the final TSH addition, the reaction was left to proceed for 2.5 hours. After 2.5 hours, the solution was hot precipitated into room temperature, stirred methanol (8x by volume). The precipitated polymer was collected by centrifugation and dried at room temperature overnight in the vacuum oven.

Characterization by Nuclear Magnetic Resonance (NMR)

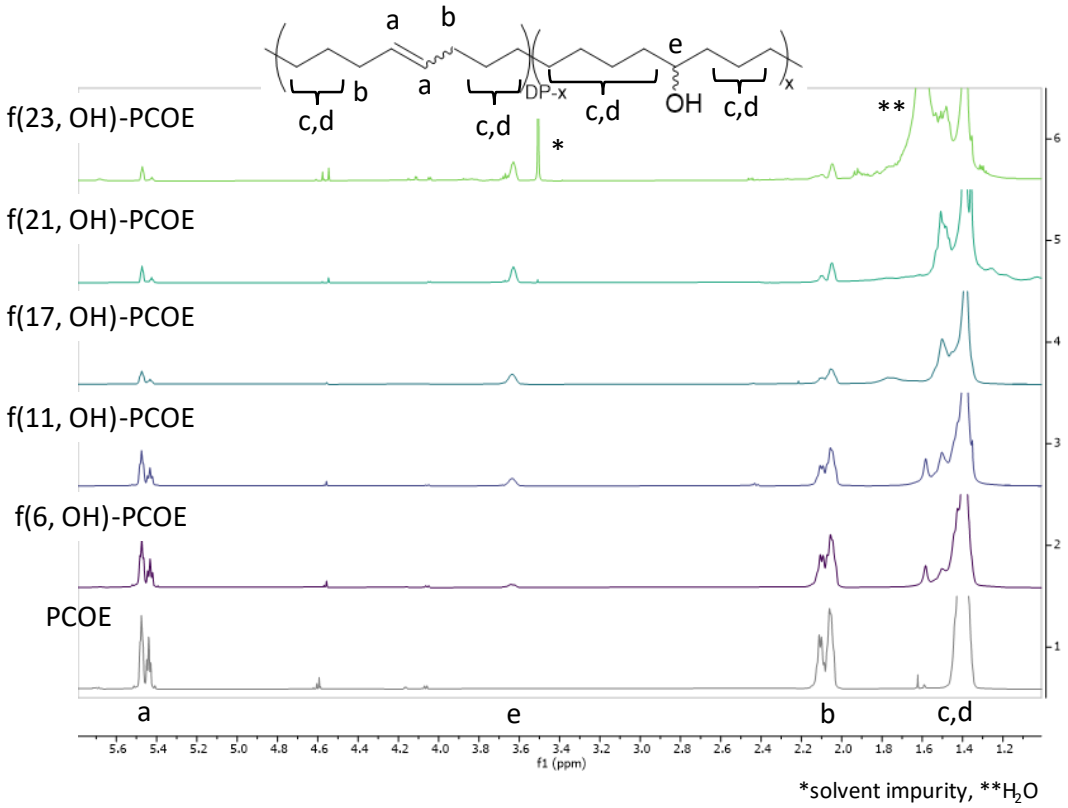

Figure S1. ^{1}H NMR of 6 to 23% functionalized f(*x*, OH)-PCOE (purple to green) shows a depletion of the vinylic resonance (a, δ 5.5 ppm) and allylic resonance (b, δ 2-2.2 ppm), with respect to the spectrum of PCOE (gray), and an appearance and growth of a new OH methanetriyl resonance (e, δ 3.6 ppm). In f(23, OH)-PCOE, the * at δ 3.5 ppm results from an NMR solvent impurity while the ** at δ 1.6 ppm is a result of residual water from precipitation.

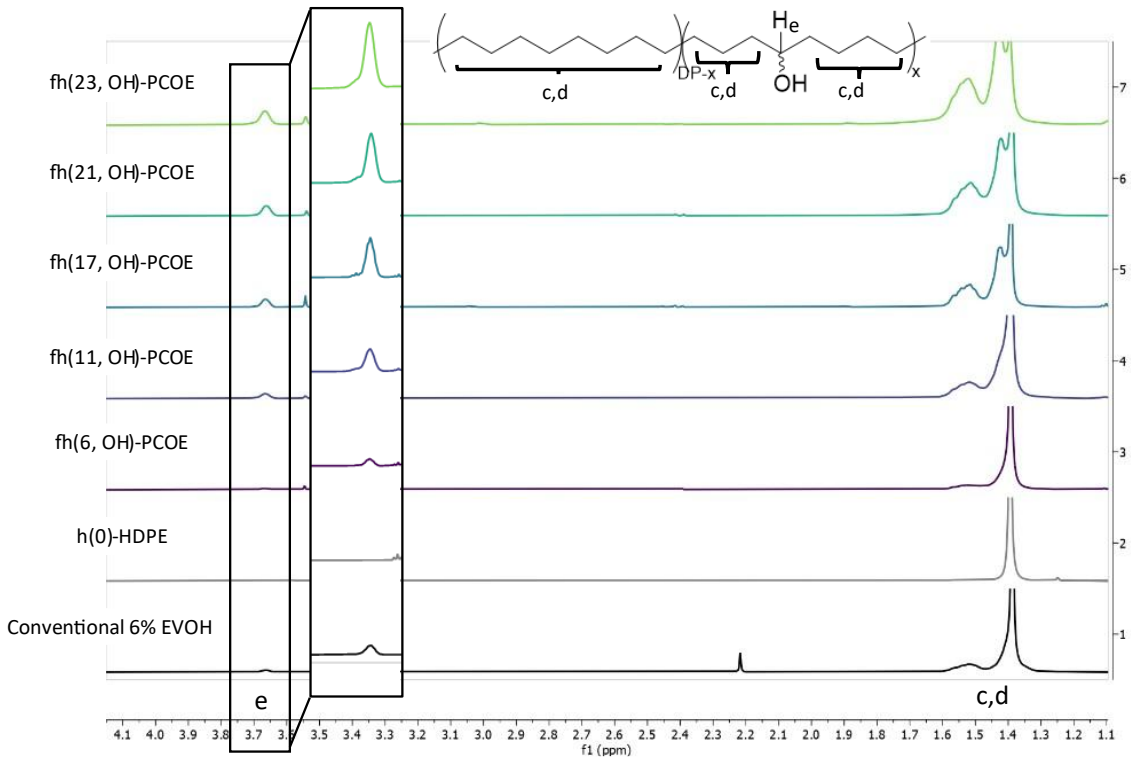

Figure S2. ^{1}H NMR of 6-23% saturated fh(*x*, OH)-PCOE (purple to green) and 6% conventional EVOH (black) have two primary resonances for the methanetriyls of the OH (e, δ ~3.65 ppm) and the aliphatic polymer backbone (c,d, δ 1.35-1.65 ppm). Fully saturated PCOE (h(0)-HDPE, gray) shows only an aliphatic resonance at δ 1.4 ppm (c,d).

Table S1. NMR Integrations for f(x,OH)-PCOE

Sample Name	Aromatic (δ 7.33 - 7.43 ppm)	Vinylic (δ 5.54 -5.35 ppm)	End-group Methylene (δ 4.62-4.50 ppm)	End-group Methylene (δ 4.10-4.00 ppm)	-OH Methanetriyl (δ 3.70-3.57 ppm)	Allylic (δ 2.15-1.99 ppm)	Aliphatic (δ 1.75-1.13 ppm)
f(0)-PCOE	0.28	2.00	0.08	0.08	-	4.13	8.31
f(6, OH)-PCOE	0.18	2.00	0.06	0.06	0.20	4.18	13.01
f(11, OH)-PCOE	0.19	2.00	0.06	0.06	0.58	4.11	20.56
f(17, OH)-PCOE	0.29	2.00	0.09	0.07	2.19	4.27	42.97
f(21, OH)-PCOE	0.49	2.00	0.18	0.18	2.90	4.98	97.44
f(23, OH)-PCOE	1.95	2.00	0.56	0.80	4.74	5.94	117.91

Table S2. NMR Integrations for fh(*x*,OH)-PCOE

Sample Name	Aromatic (δ 7.33-7.43 ppm)	End-group Methylene (δ 4.62-4.50 ppm)	-OH Methanetriyl (δ 3.70-3.57 ppm)	End-group Methylene (δ 3.60-3.56 ppm)	Aliphatic (δ 1.75-1.13 ppm)
fh(0)-PCOE	10.00	4.00	-	2.86	1044.18
fh(6, OH)-PCOE	10.00	2.23	10.71	2.47	975.69
fh(11, OH)-PCOE	10.00	1.93	28.41	2.09	1205.30
fh(17, OH)-PCOE	10.00	1.13	35.53	1.21	867.99
fh(21, OH)-PCOE	10.00	0.63	61.23	2.20	1465.24
fh(23, OH)-PCOE	10.00	0.49	53.56	-[a]	1080.99

[a]peak was indistinguishable from -OH methanetriyl

Table S3. Properties of unsaturated polymers as determined by ^{1}H NMR.

Sample	**9-BBN/Double Bond Ratio**	**Percent Functionalization (mol% vinyl alcohol)**	**Trans/Cis Ratio**	**Molecular Weight by End-Group Analysis (g/mol)**
f(0)-PCOE	-	0	62:38	5,700
f(6, OH)-PCOE	0.25:1	6	65:35	7,300
f(11, OH)-PCOE	0.50:1	11	66:34	7,300
f(17, OH)-PCOE	1.00:1	17	72:28	6,800
f(21, OH)-PCOE	1.25:1	21	73:27	4,300
f(23, OH)-PCOE	1.50:1	23	77:23	2,700

Table S4. Properties of saturated polymers as determined by ^{1}H NMR.

Sample	Percent Functionalization (mol% vinyl alcohol)	Molecular Weight by End-Group Analysis (g/mol)
h(0)-HDPE	0	6,800
fh(6, OH)-PCOE	6	7,100
fh(11, OH)-PCOE	11	9,000
fh(17, OH)-PCOE	17	6,700
fh(21, OH)-PCOE	21	11,500
fh(23, OH)-PCOE	23	8,600

End-Group Analysis (^{1}H NMR)

Molecular weight by end-group analysis is calculated using the assumption that there are two end-groups per polymer chain. The benzyloxy chain transfer agents generate C-O bonds linking the end groups to the rest of the chain. The reaction conditions under which we hydrogenate f(*x*,OH)-PCOE are known to dissociate C-O, eliminating the benzyloxy end-groups used to determine molecular weight.[1] Therefore, we attribute the apparent increase in calculated molecular weight to the loss of end-groups, **Tables S3 and S4**. Future work should investigate these chemical transformations on polymers with more stable end-groups.

Gel Permeation Chromatography

GPC was performed on polycyclooctene using an Agilent Technologies 1260 Infinity series system with two 5 μm mixed-D columns, a 5 μm guard column, a PL Gel 5 μm analytical Mixed-D column, and a RI detector (HP1047A); tetrahydrofuran (THF) was used as the eluent with a flow rate of 1.0 mL/min; polystyrene standards were used for the calibration.

Thermal Treatment/Drying of Polymer Samples

Polymers were first dried in a vacuum oven for five hours at T_m + 5 K. This drying procedure was used before FTIR, differential scanning calorimetry (DSC), X-ray scattering, contact angle, or lap joint shear.

Fourier transform infrared (FTIR) Spectroscopy

FTIR measurements were taken on a JASCO FT/IR-6800 with ATR accessory. Dried polymer powder was compressed under an anvil against a diamond crystal and ATR-FTIR measurements were conducted at 0.2 cm^{-1} resolution over 100 scans. FTIR spectra were normalized to the CH asymmetric stretching mode at ~2850 cm^{-1}, as shown in **Figure S3**. Linear growth of the OH stretching peak centered at ~3400 cm^{-1} confirms successful hydroboration/oxidation. Hydroboration/oxidation corresponded to a decrease in the C=C bending peak at ~985 cm^{-1}, **Figure S3a**. The disappearance of the C=C peak in the FTIR spectra of post-hydrogenation samples confirms successful hydrogenation.

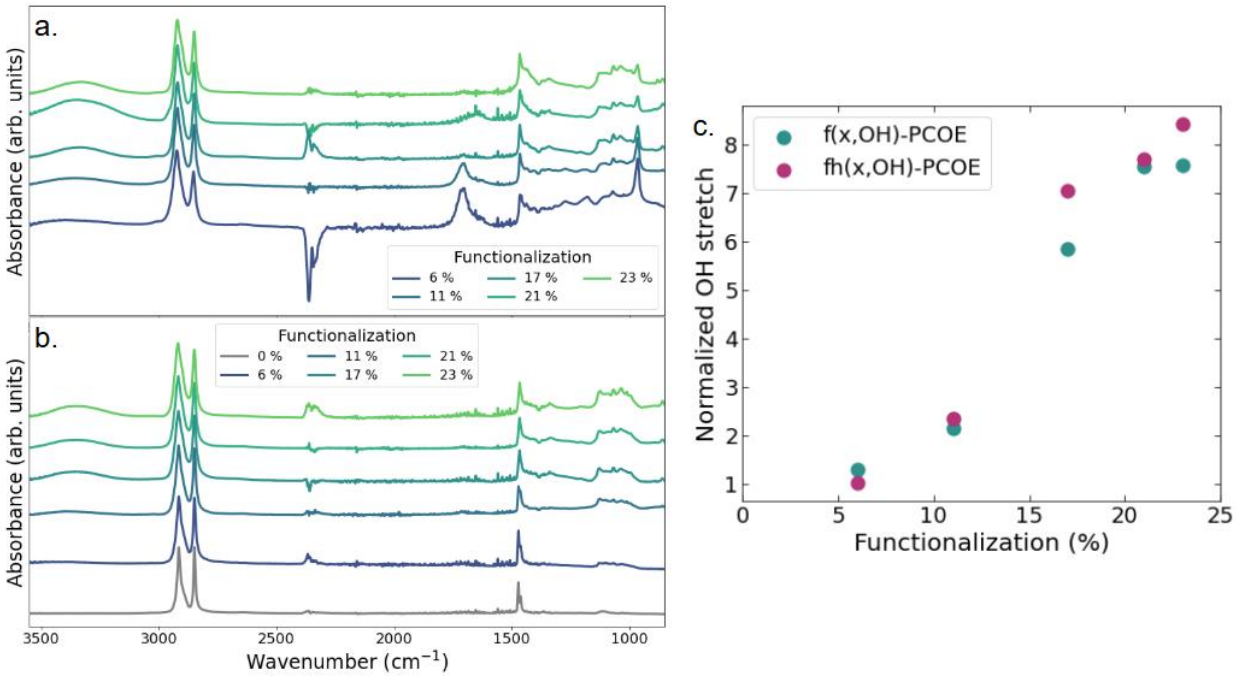

Figure S3. FTIR spectra of **(a)** f(*x*,OH)-PCOE and **(b)** fh(*x*,OH)-EVOH. The OH signal was determined by the integral of the broad peak centered at ~3400 cm^{-1} and **(c)** increased linearly with functionalization.

Prior investigations of EVOH revealed subtle shifts in the IR C-O stretch peak depending on the local environment: in the crystal (1128 cm^{-1}) or in the amorphous phase and participating (1067 cm^{-1}) or not participating (1034 cm^{-1}) in hydrogen bonding.[3–5] We observe these peaks in the fingerprint region of FTIR taken from f(*x*,OH)-PCOE and fh(*x*,OH)-PCOE, **Figure S4**.

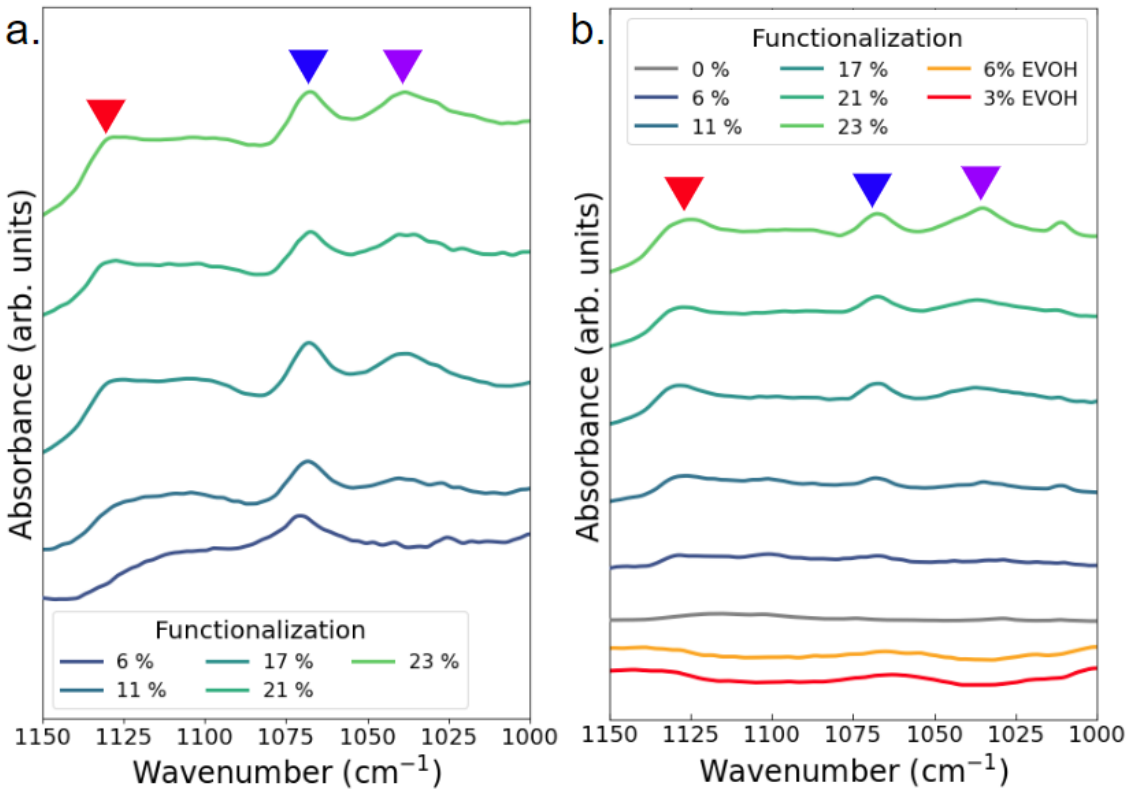

Figure S4. FTIR spectra of the C-O stretch in the fingerprint region of **(a)** f(*x*,OH)-PCOE and **(b)** fh(*x*,OH)-PCOE. The red triangle (~ 1125 cm^{-1}) marks the signal corresponding to OH in crystals; the blue triangle (~ 1070 cm^{-1}) marks the signal corresponding to OH in the amorphous phase participating in H-bonding; and the purple triangle (~ 1037 cm^{-1}) marks the signal corresponding to OH in the amorphous phase not participating in H-bonding. These peaks were not clearly observed in branched EVOH, preventing determination of the distribution of OH between the amorphous and crystalline regimes.

These peaks enable the calculation of the fraction of OH groups in the amorphous phase. After the subtraction of a Gaussian background, each peak was integrated numerically (using Simpson's rule [6]) and the resulting peak areas (A_w where w gives the wavenumber of the peak in cm^{-1}) were used to calculate the fraction of OH groups in the amorphous phase, or $f_{OH,a}$.

$$f_{OH,a} = \frac{A_{1067}+A_{1034}}{A_{1067}+A_{1034}+A_{1128}} \quad \text{(S1)}$$

The $f_{OH,a}$ values are compared both to functionalization and the amorphous fraction of the material, **Figure S5**. The amorphous fraction (f_a) was calculated from f_a = 1 - *crystallinity*. See the section

below entitled Crystallinity Calculations for more information on the determination of crystallinity.

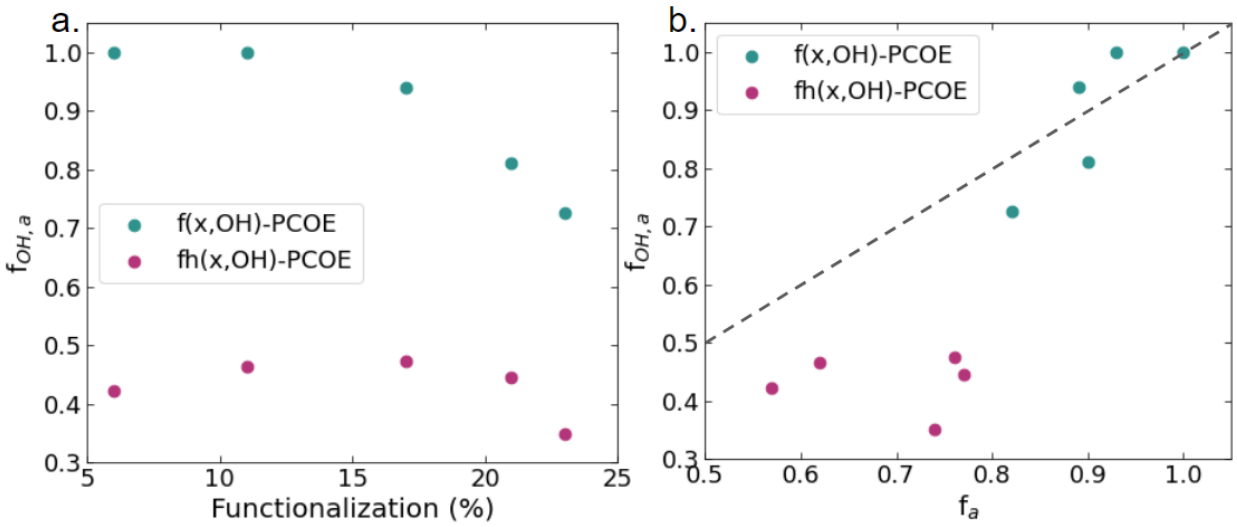

Figure S5. Fraction of OH in the amorphous phase plotted as a function of **(a)** % functionalization and **(b)** amorphous fraction of the polymer from DSC. The dashed line identifies an equal distribution of OH groups between the crystalline and amorphous phase for comparison.

Multiplying the fraction of OH in the amorphous phase by the functionalization identifies the composition of the amorphous phase in mol% OH: *Amorphous Phase OH (mol%)* = $f_{OH,a}$ x *Functionalization (mol %)*, **Figure S6**. Note that at all levels of functionalization, more OH groups are found in the amorphous phase in f(*x*,OH)-PCOE as compared to fh(*x*,OH)-PCOE.

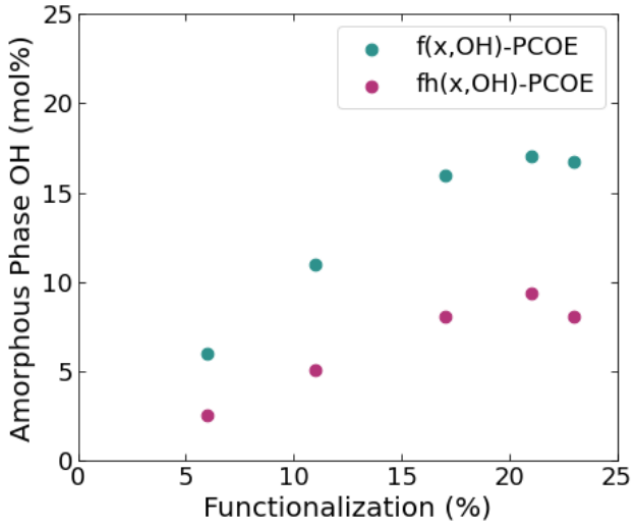

Figure S6. Amorphous phase OH (mol%) plotted against functionalization.

X-ray scattering

X-ray scattering measurements of fh(x,OH)-EVOH were conducted at 150 °C, at least 30 °C above the melting temperature for all samples, **Figure S7**. The disappearance of the scattering feature observed in room temperature measurements at low q indicates that it corresponds to the distance between OH groups within crystals.

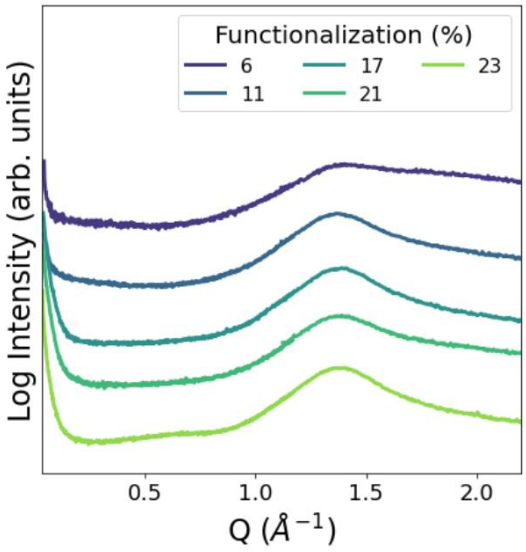

Figure S7. X-ray scattering of fh(*x*,OH)-EVOH at 150 °C.

In addition to X-ray scattering measurements on melt pressed films of all EVOH samples (both saturated and partially unsaturated), further measurements were taken on a melt pressed film of fh(23,OH)-PCOE before and after drawing (approximate strain = 50%). These measurements were taken with a SD of 177 mm so both wide and small angle features appeared on the 1M solid state detector. The 2D X-ray scattering patterns are given in **Figure S8a** and **S8b**. The drawn sample was subjected to uniaxial strain until the onset of plastic deformation and X-ray scattering was taken in the necked region, **Figure S8b**. To extract peak positions, the 2D scattering patterns are integrated azimuthally 360 degrees for the isotropic pattern (Figure S9a) and over 30-degree sectors (± 15 °) for the anisotropic pattern (**Figure S8b**) both parallel and perpendicular to the strain direction, **Figure S8c**. The peaks at 0.6 Å^{-1} correspond to a distance of ~ 1 nm correlating to the

separation between OH groups. The peaks at 1.5 $Å^{-1}$ correspond to ~ 0.4 nm and the (100) reflection of the hexagonal crystal structure. While unstrained sample exhibits an isotropic morphology, tensile deformation aligns the polymer chains in the direction of elongation with the OH spacing aligned parallel to the strain, **Figure S8b** and **S8c**. This anisotropy is further demonstrated by radial integrations showing the crystalline peak maximum 90 degrees from the layer peak maximum, **Figure S8d**.

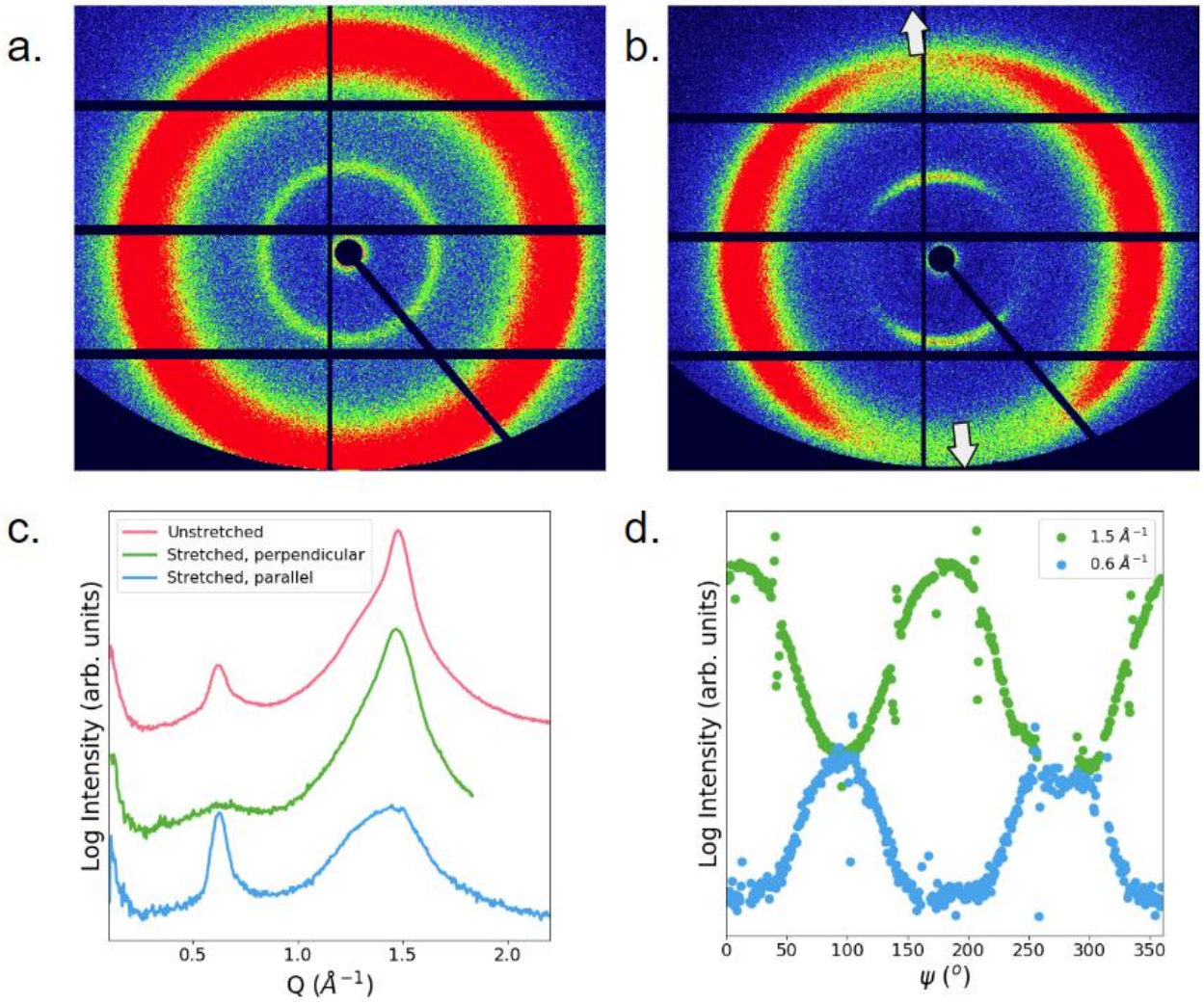

Figure S8. X-ray scattering of fh(23, OH)-EVOH **(a)** unstrained and **(b)** after uniaxial tensile deformation of ~ 50% strain in the direction of the white arrows. **(c)** Azimuthally integrated X-ray scattering traces for the unstrained sample and over 30° sectors (± 15 °) for the strained sample either perpendicular or parallel to the strain direction. **(d)** Radial integral of scattered intensity as a function of azimuthal angle for the peaks attributed to chain-chain scattering (green) or layer-like OH aggregates (blue).

Crystallinity from WAXS was identified by fitting crystalline peaks with Lorentzian functions and the amorphous halo with a double Gaussian function then dividing the integrated crystalline intensities by the total intensity (sample fit in **Figure S9**).

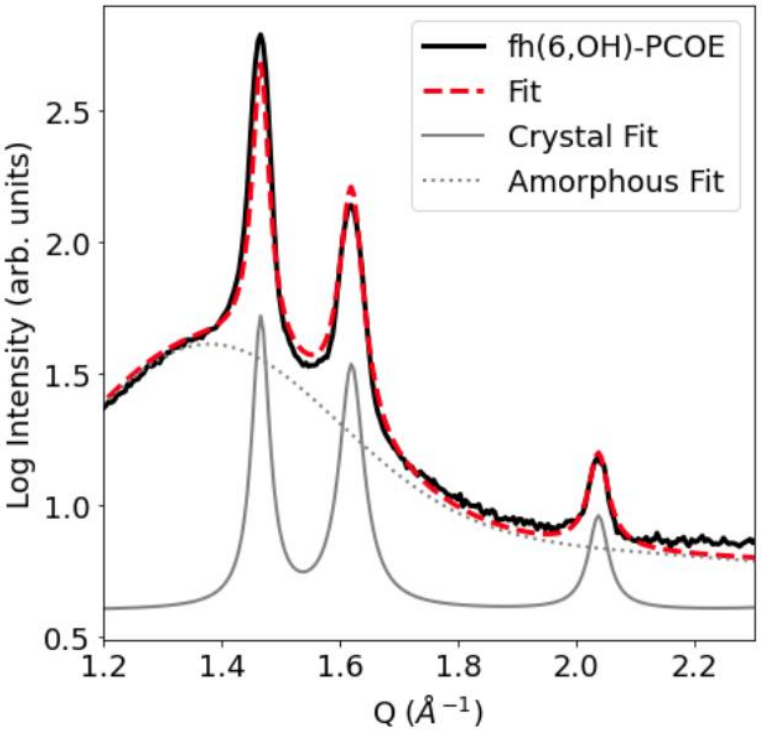

Figure S9. WAXS of fh(6,OH)-PCOE in grey with the fitting shown in red corresponding to an orthorhombic crystal. Crystalline peaks were fit to Lorentzian distributions and the amorphous background was fit to a double-Gaussian distribution. The percent crystallinity for this sample is 43%.

Thermal Properties

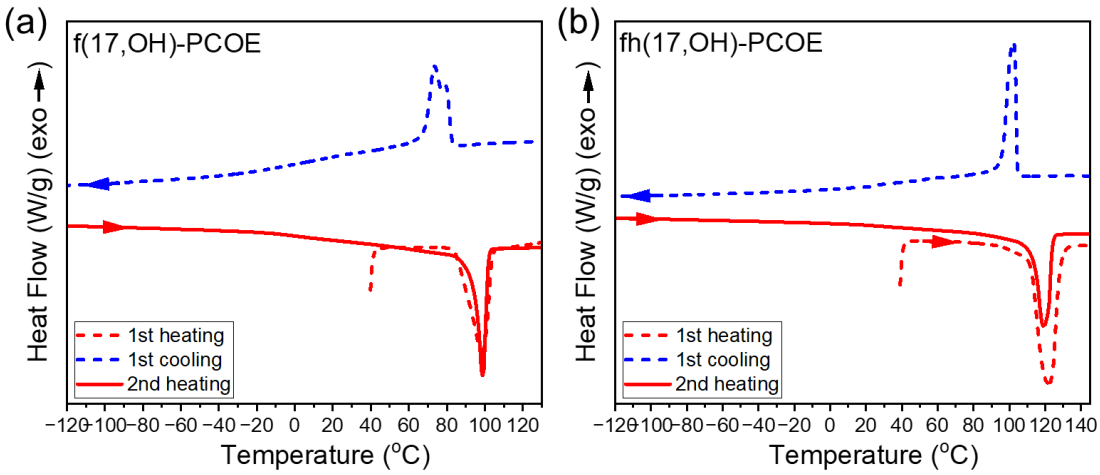

Figure S10. Sample DSC traces including the 1st heating, 1st cooling, and 2nd heating for **(a)** f(17,OH)-PCOE and **(b)** fh(17,OH)-PCOE

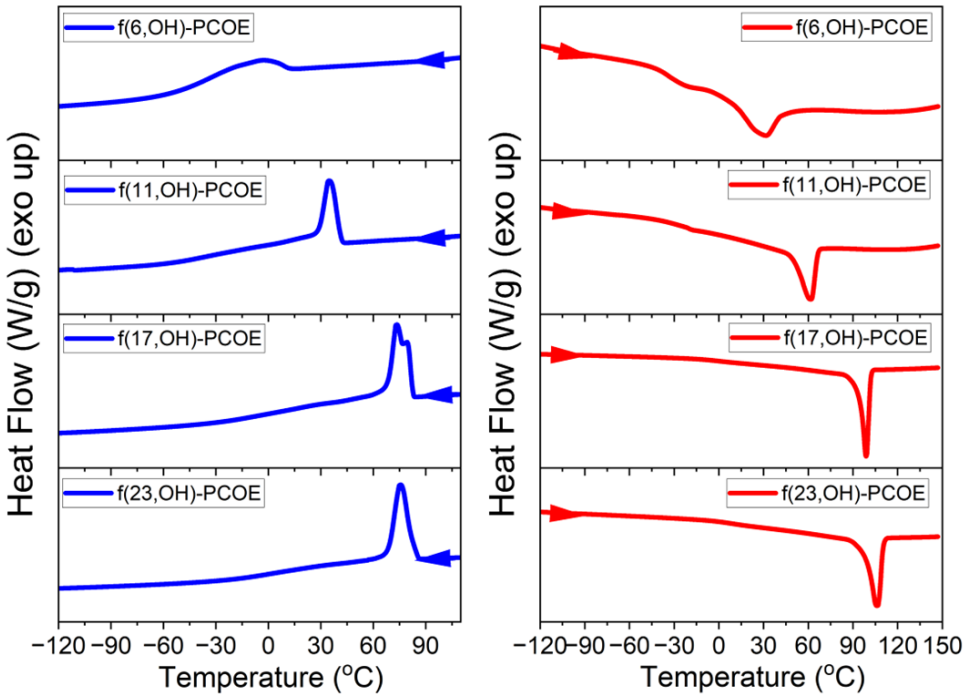

Figure S11. DSC cooling (left) and heating (right) traces showing the variation of crystallization (T_c) and melting temperature (T_m) of f(x,OH)-PCOE as a function of degree of functionalization from 6% to 23%.

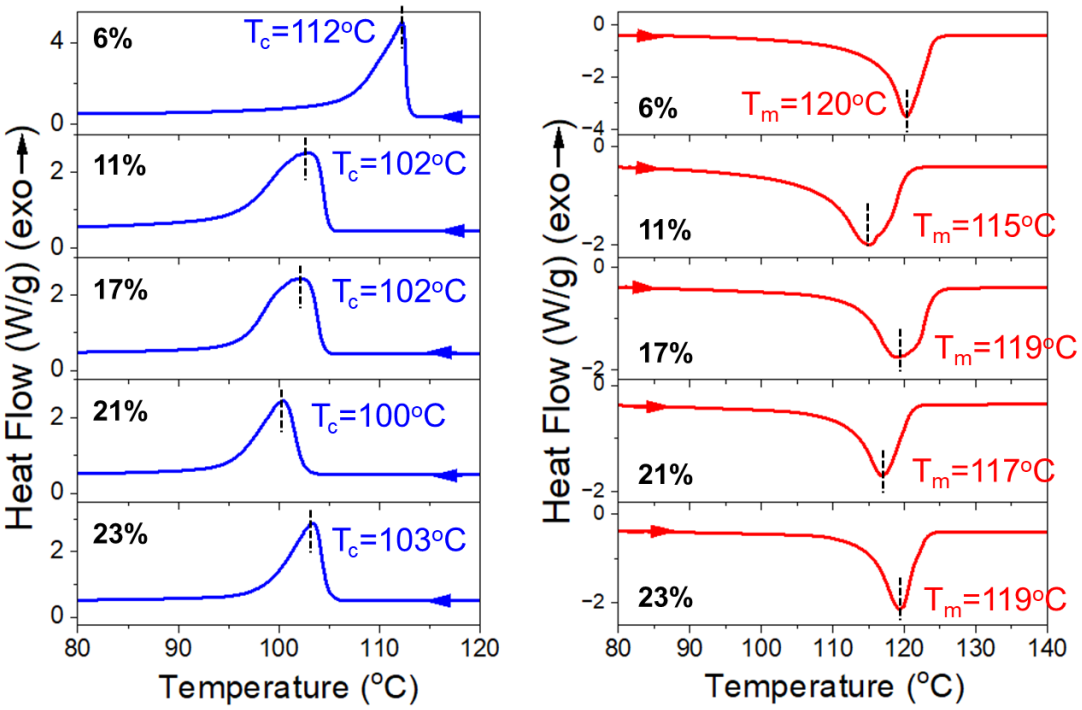

Figure S12. DSC cooling (left) and heating (right) traces showing the variation of crystallization (T_c) and melting temperature (T_m) of fh(*x*,OH)-PCOE as a function of degree of functionalization from 6% to 23%.

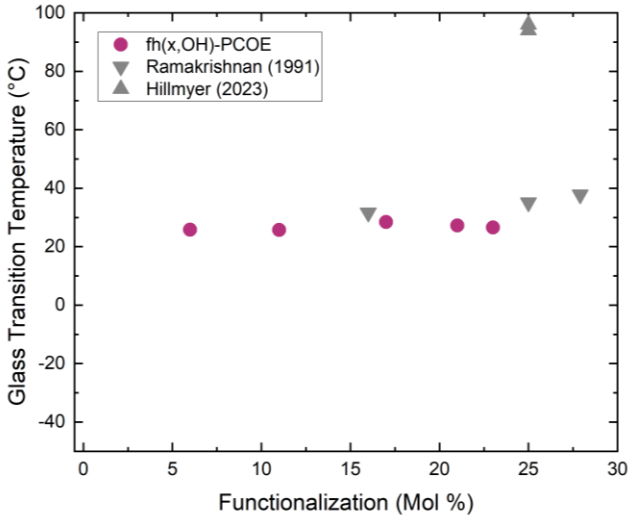

Figure S13. Glass transition temperature of fh(*x*,OH)-PCOE samples were evaluated from the second heating in DSC at 10 K/min.

Crystallinity Calculations

The percent crystallinity by DSC was calculated using

$$Percent\ Crystallinity = \frac{\Delta H_{m,DSC}}{\Delta H_m} \quad \text{(S2)}$$

Rather than use the enthalpy of melting for a homopolymer, we compute ΔH_m using a rule of mixing corresponding to the composition of the polymer. We use the tabulated values in **Table S3** for this calculation.

Table S5. Enthalpy of fusion and monomer molar mass values for the three components found in the polymer samples used for crystallinity calculations by DSC.

Component	**ΔH_m (J/g)**	**Monomer MW (M^o, g/mol)**
Polycyclooctene[7] (PCOE)	216	110.2
Poly(vinyl alcohol)[8] (PVOH)	161	44.05
Polyethylene[8] (PE)	293	28.06

Weight Fraction Calculations

The mole fraction of poly(vinyl alcohol) units in the f(*x*,OH)-PCOE polymers (*x*) was calculated from ^{1}H NMR. The mole fraction of polyethylene units and polycyclooctene units were calculated by:

$$Mol\ frac_{PE} = 3x \quad \text{(S3)}$$

$$Mol\ frac_{PCOE} = 1 - 4x \quad \text{(S4)}$$

In the saturated fh(*x*,OH)-PCOE polymers, the PCOE subunit no longer exists and therefore the *mol frac PE = 1-x*. The calculated values from Eqns S3 and S4 were then used along with the molecular weights of each monomer (M^o) to calculate the weight fraction (abbreviated to frac) of each subunit. The PCOE terms are not included in the saturated samples.

$$weight\ frac_{PCOE} = \frac{M^o_{PCOE}(1-4x)}{M^o_{PCOE}(1-4x)+3M^o_{PE}x+M^o_{PVOH}x} \quad \text{(S5)}$$

$$weight\ frac_{PE} = \frac{3M^o_{PE}x}{M^o_{PCOE}(1-4x)+3M^o_{PE}x+M^o_{PVOH}x} \quad \text{(S6)}$$

$$weight\ frac_{PVOH} = \frac{3M^o_{PE}x}{M^o_{PCOE}(1-4x)+3M^o_{PE}x+M^o_{PVOH}x} \quad \text{(S7)}$$

Enthalpy of Melting for Unsaturated Samples (f(x,OH)-PCOE):

$$\Delta H_m(x) = \left(\Delta H_{m,PCOE} \times weight\ frac_{PCOE}\right) + \left(\Delta H_{m,PVOH} \times weight\ frac_{PVOH}\right) + \left(\Delta H_{m,PE} \times weight\ frac_{PE}\right) \quad \text{(S8)}$$

Enthalpy of Melting for Saturated Samples (fh(x,OH)-PCOE):

$$\Delta H_m(x) = \left(\Delta H_{100,PVOH} \times weight\ frac_{PVOH}\right) + \left(\Delta H_{100,PE} \times weight\ frac_{PE}\right) \quad \text{(S9)}$$

Table S6. Thermal values and crystallinity extracted from DSC and WAXS for f(x,OH)-PCOE and fh(x,OH)-PCOE.

Sample	T_g (°C)	T_m (°C)	X_c (by DSC) (%)	X_c (by WAXS) (%)

f(6,OH)-PCOE	-33.0	31.3	4	0
f(11,OH)-PCOE	-25.1	61.7	10	7
f(17,OH)-PCOE	-0.4	98.8	21	11
f(21,OH)-PCOE	-	-	-	10
f(23,OH)-PCOE	9.5	106	17	18
fh(6,OH)-PCOE	25.8	120.3	46	43
fh(11,OH)-PCOE	25.7	115.3	35	38
fh(17,OH)-PCOE	28.5	117.3	25	24
fh(21,OH)-PCOE	27.2	116.9	18	23
fh(23,OH)-PCOE	26.6	119.3	21	26

Surface and Mechanical Properties

Contact angle measurements

Water contact angle measurements were performed by applying a 10 μL droplet to the surface of a hot pressed polymer film. The profile of the droplet was photographed then fit with the Young-Laplace equation to identify contact angle, Eqn S10, where *r* gives the radius of the droplet at the intersection with the surface, α is the contact angle, *b* gives the radius of curvature at the maximum height, and *c* is the capillary constant at the surface.[9]

$$c(b - r\cos\alpha) + \frac{2}{b} = \frac{2r^2 + 3r'^2 - rr'' - (\frac{1}{\tan\alpha})(\frac{r'^3}{r} + r'r)}{(r'^2 + r^2)^{3/2}} \quad \text{(S10)}$$

Lap joint shear

To confirm that hot pressing, lap joint annealing, and lap joint shear tests do not alter the C=C bonds in the f(*x*,OH)-PCOE samples, we performed FTIR on films recovered after lap joint shear testing (or post-LJS). Comparing the integrated intensity of the C=C bending peak supports the stability of unsaturations throughout film preparation and characterization, **Figure S14.**

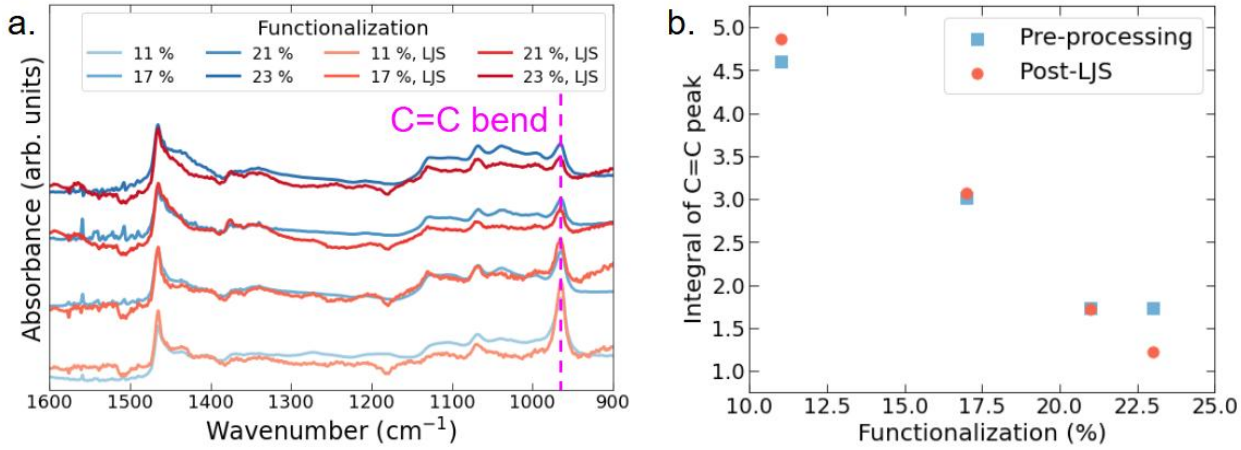

Figure S14. (a) FTIR of unsaturated f(*x*,OH)-PCOE before processing (blue) and on films recovered post-lap joint shear (red). **(b)** Integrated intensity of C=C bending peak for samples both before processing and post-LJS.

Note that lap joints of PCOE with no functionalization (both unsaturated and saturated) were prepared but broke immediately upon loading onto the Instron.

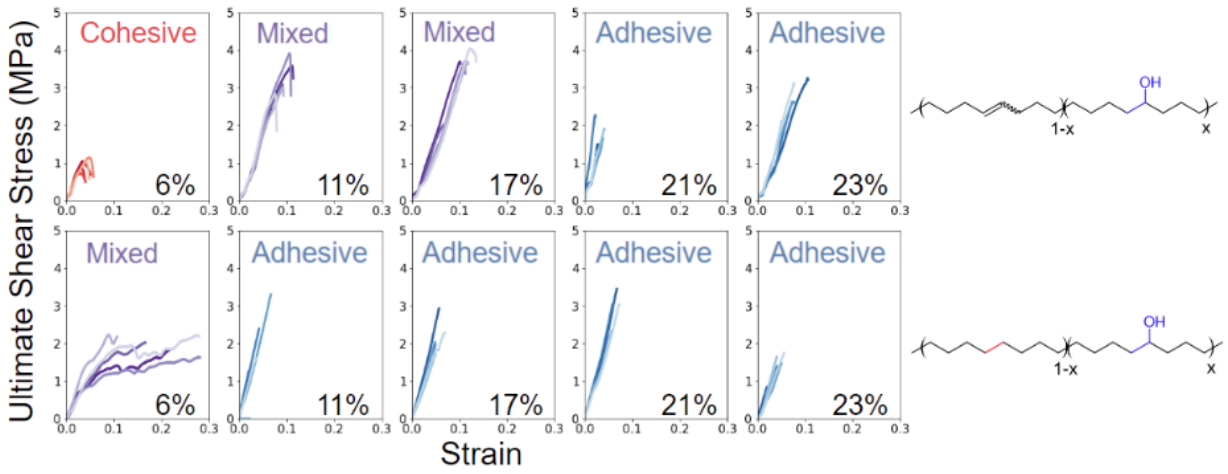

Figure S15. Stress-strain curves from five replicates of lap joint shear measurements of alcohol functionalized polymers f(*x*,OH)-PCOE (top) and fh(*x*,OH)-PCOE (bottom). Samples that failed in cohesion are shown in red; samples with mixed failure modes are shown in purple; and samples that failed in adhesion are shown in blue.

Dielectric spectroscopy (DS)

The dynamical properties of each relaxation process are extracted via empirical Havriliak-Negami (HN) functions on the imaginary part of the complex dielectric permittivity:

$$\varepsilon^*_{HN}(\omega,T) = \varepsilon_\infty(T) + \sum_{k=1}^{2\ or\ 3} \frac{\Delta\varepsilon_k(T)}{\left[1+\left(i\omega\tau_{HN,k}(T)\right)^a\right]^b} + \frac{\sigma_0(T)}{i\varepsilon_0\omega} \quad \text{(S11)}$$

with

$$\tau_{max} = \tau_{HN}\left[\sin\left(\frac{ab\pi}{2b+2}\right)\right]^{\frac{1}{a}}\left[\sin\left(\frac{a\pi}{2b+2}\right)\right]^{-\frac{1}{a}} \quad \text{(S12)}$$

where ε_∞ is the dielectric permittivity at the limit of high frequencies, $\Delta\varepsilon$ is the dielectric intensity, τ_{HN} the HN relaxation time, a, b (with limits of $0 < a$, $ab \leq 1$) are shape parameters describing the dynamic heterogeneity (a and ab are the slopes of low frequency region and high frequency region, respectively), σ_0 is the dc conductivity, ε_0 is the vacuum permittivity, and $\sigma_0/(\omega\varepsilon_0)$ is the conductivity term accounting for the upturn in ε'' at low frequency and high temperatures.

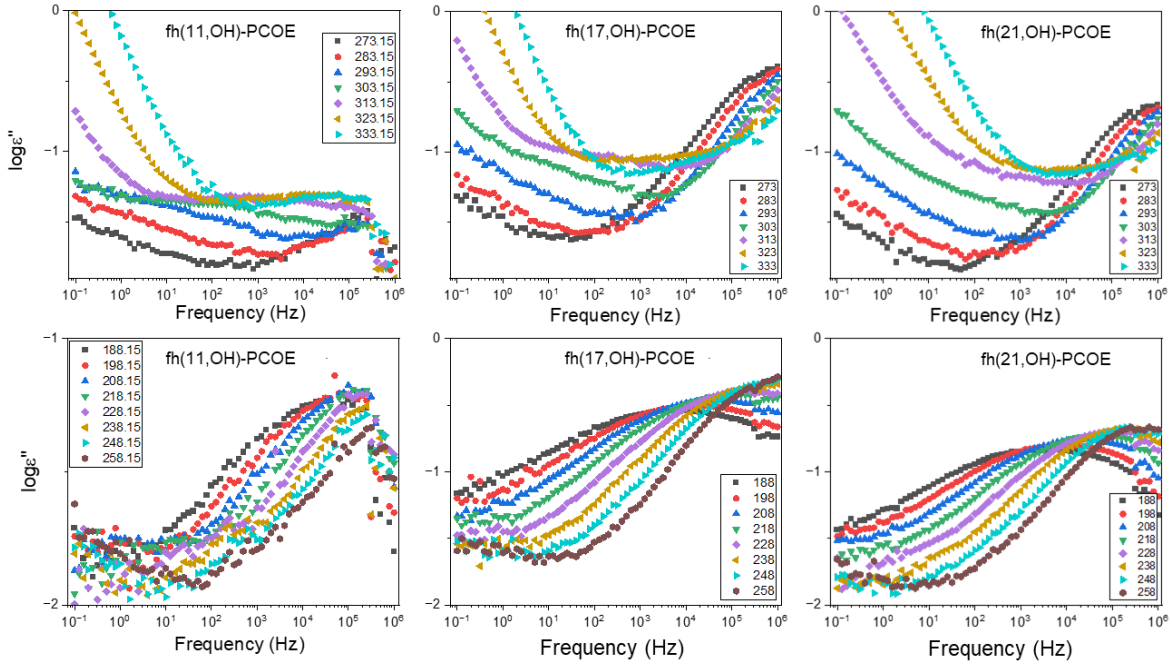

Figure S16. Representative dielectric loss (ε'') spectra for the fh(x,OH)-PCOE at higher temperatures (top row) and lower temperatures (bottom row), corresponding to the segmental and subsegmental dynamics, respectively.

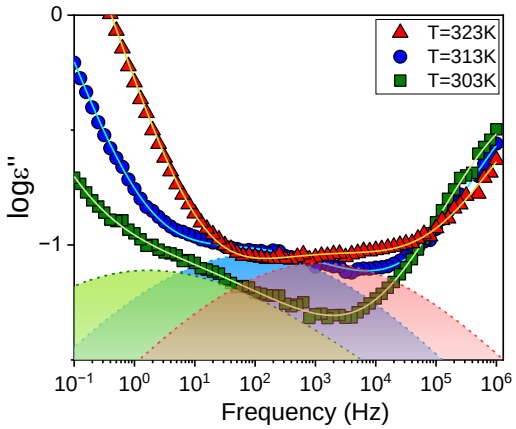

Figure S17. Representative HN function fittings to logarithmic dielectric loss spectra of fh(17,OH)-PCOE: (green squares) 303 K, (blue circles) 313 K, and (red triangles) 323 K. Solid lines represent the summation of three HN function fittings. The dashed lines with shaded area indicate the dielectric α-process or segmental dynamics.

Table S7. Activation energies of unsaturated and saturated polymer samples as calculated from dielectric spectroscopy measurements

Sample	Activation Energy (E_a, kJ/mol)
f(11, OH)-PCOE	15.6 ± 0.4
f(17, OH)-PCOE	17.6 ± 0.1
f(21, OH)-PCOE	18.2 ± 0.2
fh(11, OH)-PCOE	7.7 ± 0.5
fh(17, OH)-PCOE	13.1 ± 0.1
fh(21, OH)-PCOE	13.5 ± 0.1

References

(1) Hahn, S. F. An Improved Method for the Diimide Hydrogenation of Butadiene and Isoprene Containing Polymers. *J. Polym. Sci. A Polym. Chem.* **1992**, *30* (3), 397–408. https://doi.org/10.1002/pola.1992.080300307.

(2) Mango, L. A. Mechanism and Stereochemistry in the Anionic Polymerization of 1, 3-Cyclohexadiene and the Diimide Hydrogenation of Polymers/, University of Massachusetts Amherst, 1972. https://doi.org/10.7275/NRD6-SZ36.

(3) Finch, C. A.; Dunn, A. *Polyvinyl Alcohol--Developments*, 2nd Edition.; John Wiley & Sons, Inc.: Hoboken, New Jersey, U.S., 1992.

(4) Xu, W.; Asai, S.; Sumita, M. Spectroscopic Study of Ethylene Vinyl Alcohol Copolymer and Poly (Vinyl Alcohol). *SEN'I GAKKAISHI* **1997**, *53* (5), 174–182. https://doi.org/10.2115/fiber.53.5_174.

(5) Takahashi, M.; Tashiro, K.; Amiya, S. Crystal Structure of Ethylene−Vinyl Alcohol Copolymers. *Macromolecules* **1999**, *32* (18), 5860–5871. https://doi.org/10.1021/ma990521a.

(6) McKeeman, W. M. Algorithm 145: Adaptive Numerical Integration by Simpson's Rule. *Commun. ACM* **1962**, *5* (12), 604. https://doi.org/10.1145/355580.369102.

(7) Schneider, W. A.; Müller, M. F. Crystallinity of Trans-Polyoctenamer: Characterization and Influence of Sample History. *Journal of Molecular Catalysis* **1988**, *46* (1), 395–403. https://doi.org/10.1016/0304-5102(88)85111-3.

(8) Blaine, R. *Polymer Heats of Fusion*; Thermal Applications Note TN048; TA instruments. https://www.tainstruments.com/pdf/literature/TN048.pdf (accessed 2024-05-20).

(9) Stadler, F. J.; Bailly, C. A New Method for the Calculation of Continuous Relaxation Spectra from Dynamic-Mechanical Data. *Rheol Acta* **2009**, *48* (1), 33–49. https://doi.org/10.1007/s00397-008-0303-2.